Atmospheric
Chemistry
and Physics
Discussions

Open Access

Kerb and urban increment of highly time-resolved trace elements in PM$_{10}$, PM$_{2.5}$ and PM$_{1.0}$ winter aerosol in London during ClearfLo 2012

S. Visser[1], J. G. Slowik[1], M. Furger[1], P. Zotter[1], N. Bukowiecki[1], R. Dressler[2], U. Flechsig[3], K. Appel[4,*], D. C. Green[5], A. H. Tremper[5], D. E. Young[6], P. I. Williams[6,7], J. D. Allan[6,7], S. C. Herndon[8], L. R. Williams[8], C. Mohr[9], L. Xu[10], N. L. Ng[10,11], A. Detournay[12], J. F. Barlow[13], C. H. Halios[13], Z. L. Fleming[7,14], U. Baltensperger[1], and A. S. H. Prévôt[1]

[1]Laboratory of Atmospheric Chemistry, Paul Scherrer Institute, Villigen, Switzerland
[2]Laboratory of Radiochemistry and Environmental Chemistry, Paul Scherrer Institute, Villigen, Switzerland
[3]Swiss Light Source, Paul Scherrer Institute, Villigen, Switzerland
[4]HASYLAB, DESY Photon Science, Hamburg, Germany
[5]School of Biomedical Sciences, King's College London, London, UK
[6]School of Earth, Atmospheric and Environmental Sciences, University of Manchester, Manchester, UK

[7]National Centre for Atmospheric Science, University of Manchester, Manchester, UK
[8]Aerodyne Research, Inc., Billerica, MA, USA
[9]Department of Atmospheric Sciences, University of Washington, Seattle, WA, USA
[10]School of Chemical and Biomolecular Engineering, Georgia Institute of Technology, Atlanta, GA, USA
[11]School of Earth and Atmospheric Sciences, Georgia Institute of Technology, Atlanta, GA, USA
[12]Centre for Ecology and Hydrology, Penicuik, Midlothian, Scotland
[13]Department of Meteorology, University of Reading, Reading, UK
[14]Department of Chemistry, University of Leicester, Leicester, UK
[*]now at: European XFEL, Hamburg, Germany

Correspondence to: M. Furger (markus.furger@psi.ch)

Title Page

Abstract | Introduction

Conclusions | References

Tables | Figures

|◄ | ►|

◄ | ►

Back | Close

Full Screen / Esc

Printer-friendly Version

Interactive Discussion

Full Screen / Esc

Printer-friendly Version

Interactive Discussion

Abstract

Ambient concentrations of trace elements with 2 h time resolution were measured in $PM_{10-2.5}$, $PM_{2.5-1.0}$ and $PM_{1.0-0.3}$ size ranges at kerbside, urban background and rural sites in London during winter 2012. Samples were collected using rotating drum impactors (RDIs) and subsequently analysed with synchrotron radiation-induced X-ray fluorescence spectrometry (SR-XRF). Quantification of kerb and urban increments (defined as kerb-to-urban and urban-to-rural concentration ratios, respectively), and assessment of diurnal and weekly variability provided insight into sources governing urban air quality and the effects of urban micro-environments on human exposure. Traffic-related elements yielded the highest kerb increments, with values in the range of 11.6 to 18.5 for SW winds (3.6–9.4 for NE) observed for elements influenced by brake wear (e.g. Cu, Sb, Ba) and 5.6 to 8.0 for SW (2.6–6.5 for NE) for other traffic-related processes (e.g. Cr, Fe, Zn). Kerb increments for these elements were highest in the $PM_{10-2.5}$ mass fraction, roughly 3 times that of the $PM_{1.0-0.3}$ fraction. These elements also showed the highest urban increments (~ 3.0), although no difference was observed between brake wear and other traffic-related elements. Traffic-related elements exhibited higher concentrations during morning and evening rush hour, and on weekdays compared to weekends, with the strongest trends observed at the kerbside site, and additionally enhanced by winds coming directly from the road, consistent with street canyon effects. Elements related to mineral dust (e.g. Al, Ca, Sr) showed significant influences from traffic-induced resuspension, as evidenced by moderate kerb (2.0–4.1 for SW, 1.4–2.1 for NE) and urban (1.7–2.3) increments and increased concentrations during peak traffic flow. Elements related to regional transport showed no significant enhancement at kerb or urban sites, with the exception of $PM_{10-2.5}$ sea salt (factor of 1.5–2.0), which may be influenced by traffic-induced resuspension of sea and/or road salt. Heavy duty vehicles appeared to have a larger effect than passenger vehicles on the concentrations of all elements influenced by resuspension (including sea salt) and wearing processes. Trace element concentrations in London were

influenced by both local and regional sources, with coarse and intermediate fractions dominated by traffic-induced resuspension and wearing processes and fine particles influenced by regional transport.

1 Introduction

Ambient particulate matter (PM) has long been recognized to have a detrimental effect on public health in urban areas (e.g. Dockery and Pope, 1994). Of particular interest are particles with an aerodynamic diameter less than 10 µm (PM_{10}) as these particles can penetrate deeply into the lungs (Franklin et al., 2008; Zhou et al., 2011). Reche et al. (2012) showed even higher toxicity to human cells for the $PM_{2.5-1.0}$ than for the $PM_{10-2.5}$ fraction. Particle toxicity is known to vary significantly with PM composition and emission sources (Kelly and Fussell, 2012), with identified toxic constituents including soluble secondary inorganic particles, elemental and organic carbon, and especially metals. Effective mitigation strategies therefore require detailed, size-dependent characterization of particle composition and emission sources.

In addition to their direct effects on human health, metals and trace elements are of importance because their high source specificity and atmospheric stability make them effective tracers for source apportionment. In Europe, four main source types in PM_{10} are commonly identified: vehicles (including e.g. Fe, Ba, Zn, Cu), crustal materials (e.g. Al, Si, Ca, Fe), sea salt (mainly Na, Cl, Mg) and mixed industrial/fuel-oil combustion (mainly V, Ni, S) and secondary aerosol (mainly S) (Putaud et al., 2010; Viana et al., 2008). The contribution of mineral dust and sea salt in most urban areas is larger in PM_{10} than in $PM_{2.5}$ (Harrison et al., 2001; Weijers et al., 2011). Emissions from vehicle exhaust, industry and secondary aerosol are predominantly emitted and formed as $PM_{1.0}$ or in $PM_{2.5}$ (Bukowiecki et al., 2010; Harrison et al., 2011; Richard et al., 2011). Several of these sources have been directly linked to adverse health effects. For example, the largest aerosol source of human toxicity in Barcelona was attributed to traffic activities (encompassing vehicle emissions, road dust and secondary nitrate),

with fuel oil combustion and industrial emissions also contributing to increased cancer risk (Reche et al., 2012). Turoczi et al. (2012) observed higher toxicity from direct emissions (e.g. from traffic) than from photochemically processed aerosol.

The Clean Air for London project (ClearfLo; www.clearflo.ac.uk) is a multinational effort to elucidate the processes driving poor air quality in London, implemented through comprehensive measurements of particle- and gas-phase composition, as well as meteorological parameters (Bohnenstengel et al., 2013a). ClearfLo builds upon recent modelling and monitoring studies in London (Arnold et al., 2004; Bohnenstengel et al., 2011, 2013b; Harrison et al., 2012a; Mavrogianni et al., 2011). Despite improved air quality, PM_{10} concentrations are not falling, resulting in frequent exceedances of the daily PM_{10} limit (Harrison et al., 2008). Such exceedances are caused by complex interactions of regional and local emission sources, together with meteorological factors such as wind speed, air mass origin, and daily cycles of the atmospheric boundary layer (Charron and Harrison, 2005; Harrison and Jones, 2005; Jones et al., 2010). Currently, emissions by industrial sources and stationary combustion are modest, however, traffic contributes up to 80 % of the total PM_{10} in London, compared to less than 20 % for the entire UK, according to emission inventories between 1970 and 2001 (Dore et al., 2003).

The spatial density of emission sources found in typical urban environments leads to elevated particle concentrations compared to nearby rural locations. Buildings, e.g., may influence local meteorology by restricting air circulation (street canyon effect), producing human exposures that are orders of magnitude higher than those predicted by regional dispersion models (Zhou and Levy, 2008). This provides both acute exposure risk and increased long-term exposure for those passing through regularly, thereby producing a non-negligible impact on public health. To assess the impact of such microenvironments, we here investigate London trace element concentrations in terms of increments, defined as the concentration ratios between an environment of interest and a reference site (e.g. Charron et al., 2007).

Only a few studies have investigated trace elements through simultaneous measurements at urban background and rural or kerbside sites. Harrison et al. (2012b) report increments of kerbside to urban background sites in London for non-size segregated aerosol with a time resolution of 1 to 4 days in London. Theodosi et al. (2011) found that at urban and suburban sites in Athens and a regional site in Finokalia, Greece crustal elements dominate the coarse mode ($PM_{10-2.5}$), whereas anthropogenic sources such as fossil fuel combustion were confined in the fine mode (V, Ni and Pb have $> 70\%$ of their mass in $PM_{1.0}$). Bukowiecki et al. (2009a, 2010) examined trace elements in $PM_{10-2.5}$, $PM_{2.5-1.0}$ and $PM_{1.0-0.1}$ aerosol at street canyon and urban background sites in Zürich, Switzerland, and showed increasing increments (note: 1 means no increment) with particle size from about 1.2 (fine mode) to 2.4 (coarse mode) (averaged over all elements). All these studies report increments close to 1 for elements originating from regional sources such as sea salt and Saharan dust, while local, especially traffic-related sources yield increments around 2 for resuspension-related elements and between 3 and 5 for traffic-related elements. Additionally, the 1 h time resolution used by Bukowiecki et al. (2009a, 2010) enabled identification of enhanced increments for resuspension and wearing related elements like Si and Sb during peak traffic flows.

There is a need for more high time-resolved size segregated increment analyses to assess the exposure to trace elements from emission sources within urban areas under varying meteorological conditions. Here we present size segregated ($PM_{10-2.5}$, $PM_{2.5-1.0}$ and $PM_{1.0-0.3}$) measurements of aerosol trace elements with 2 h time resolution performed simultaneously at kerbside and urban background sites in London, and at a rural site outside London during the winter intensive field campaign of ClearfLo. We assess the effects of urban micro-environments on human exposure to particulate pollutants through the quantification of urban and kerb increments. These exposures are further investigated in terms of contributing emission sources, diurnal and weekly variability, local wind patterns, and regional transport effects.

2 Methods

2.1 Measurement campaigns

The ClearfLo project was a measurement program in and around London lasting two years (2011–2012) and including two month-long Intensive Observation Periods (IOPs) in 2012 (Bohnenstengel et al., 2013a). This paper focuses on the winter IOP lasting from 6 January to 11 February 2012. Measurements took place at three sampling sites located at or near permanent air quality measurement stations in the Automatic Urban and Rural Network (AURN): a kerbside site close to a very busy road, an urban background site in a residential area, and a rural background site away from direct emission sources (see Fig. 1).

The urban background sampling site was at the grounds of the Sion Manning Secondary School in North Kensington (NK, lat 51°31′21″ N, lon 0°12′49″ W). NK is situated within a highly trafficked suburban area of London (Bigi and Harrison, 2010; Harrison et al., 2012a). During the ClearfLo IOPs this site served as the main measurement site and was upgraded with a full suite of particle- and gas-phase instruments, as well as instruments to measure meteorological parameters (Bohnenstengel et al., 2013a). The kerbside site was located at Marylebone Road (MR, lat 51°31′21″ N, lon 0°09′17″ W) about 4.1 km to the east of NK (Charron and Harrison, 2005; Harrison et al., 2011). This site is located at the southern side of a street canyon, with an axis running approximately 260° to 80°. Measurements took place at 1 m from a busy six-lane road with a traffic flow of approximately 73 000 vehicles per day of which 15 % consists of heavy duty vehicles (trucks and buses). Braking and stationary vehicle queues are frequent at the site due to a heavily used pedestrian light-controlled crossing (65 m west of MR) and a signal-controlled junction (200 m west of MR). The rural site at the Kent Showgrounds at Detling (DE, lat 51°18′07″ N, lon 0°35′22″ E) is situated approximately 45 km to the southeast of London downtown on a plateau at 200 m a.s.l. surrounded by fields and villages, and is close to the permanent measurement station of Kent and Medway Air Quality Monitoring Network. The site provides excellent

opportunities to compare the urban and kerbside air pollution with the rural background pollution levels (Bohnenstengel et al., 2013a; Mohr et al., 2013). A busy road with ~ 160 000 vehicles per day (traffic fleet composition unknown) is located approximately 150 m south of DE. Meteorological parameters were measured at DE and at the British Telecom (BT) Tower (lat 51°31′17″ N, lon 0°08′20″ W), ~ 0.5 km east of MR (Harrison et al., 2012a).

2.2 Instrumentation

2.2.1 RDI-SR-XRF

Rotating drum impactors

Rotating drum impactors (RDIs) were deployed at MR, NK and DE with a 2 h time resolution (see Table 1 for details). A detailed description of the RDI can be found in Bukowiecki et al. (2005, 2009c) and Richard et al. (2010). In short, aerosols are sampled through an inlet that removes all particles with diameter $d > 10\,\mu\text{m}$ at a flow rate of $1\,\text{m}^3\,\text{h}^{-1}$. The particles are size segregated in three size ranges based on aerodynamic diameter ($PM_{10-2.5}$ (coarse), $PM_{2.5-1.0}$ (intermediate) and $PM_{1.0-0.3}$ (fine)) by passing sequentially through three rectangular nozzles of decreasing size (width 1.52, 0.68 and 0.3 mm, length 10 mm). Particle deposition occurs via impaction on a 6 μm thick polypropylene (PP) foil mounted on aluminium wheels and coated with Apiezon to minimize particle bouncing effects. After the last impaction stage a backup filter samples all remaining particles before the air passes through a pump. After each 2 h sampling interval the three wheels rotate stepwise to a blank section of the foil before a new sampling interval takes place. The small-size collection limit of the fine fraction was previously estimated at 100 nm (Bukowiecki et al., 2009c; Richard et al., 2010). However, new laboratory measurements of the RDI collection efficiency indicate an instrument-dependent (i.e. based on the machining of the specific nozzle) small-end cut point of approximately 290–410 nm (see Supplement A for details). This results in

an underestimation of the total mass of trace elements that occur predominantly in the $PM_{1.0}$ fraction, notably S, K and Pb.

SR-XRF analysis

Trace element analysis on the RDI samples was performed with synchrotron radiation-induced X-ray fluorescence spectrometry (SR-XRF) at the X05DA beamline (Flechsig et al., 2009) at the Swiss Light Source (SLS) at Paul Scherrer Institute (PSI), Villigen PSI, Switzerland and at Beamline L at Hamburger Synchrotronstrahlungslabor (HASYLAB) at Deutsches Elektronen-Synchrotron (DESY), Hamburg, Germany (beamline dismantled November 2012). The RDI samples with the deposited particles were placed directly into the X-ray beam. Irradiation of the samples took place at a 45° angle for 30 s. The light spot of the incoming beam was ∼ 140 by 70 μm at SLS (monochromatic excitation at 10.5 keV, in vacuum) and ∼ 80 by 150 μm at HASYLAB (polychromatic excitation, in air). Fluorescence light produced by the elements in the samples was detected by energy-dispersive detectors (silicon drift detector at SLS, nitrogen cooled Si(Li)-detector at HASYLAB) at a 90° angle relative to the incoming beam. At SLS Kα lines of the elements with atomic number Z = 11–30 (Na-Zn) were measured and at HASYLAB Kα lines of the elements with Z = 22–56 (Ti-Ba) and Lα lines of Z = 82 (Pb).

The fluorescence counts per element were calibrated to the element mass concentration using multi-element standards, where each standard consisted of a set of preselected elements in 5 different concentrations ranging between 0.05 and 0.4 μg cm^{-2}. The absolute element concentrations in these standards were determined with inductively coupled plasma-optical emission spectroscopy (ICP-OES). The absolute calibration factor for the SR-XRF system was referenced to Fe and determined from the linear relation between the SR-XRF response and the ICP-OES measurements. Because the fluorescence yield increases with atomic number Z, a relative calibration curve was constructed as follows: for each element present in the standards and having a detectable Kα_1 line, an absolute calibration factor was determined as for Fe, and

Title Page

Abstract | Introduction

Conclusions | References

Tables | Figures

Back | Close

Full Screen / Esc

Printer-friendly Version

Interactive Discussion

a dimensionless relative response factor was calculated as the ratio of this absolute factor to that of Fe. These relative response factors were plotted as a function of line energy and the curve was fit by a custom function that smoothly blends exponential (low energy) and sigmoidal (high energy) functions. The response curve was interpolated to obtain response factors for elements not present in the standard. In total 25 elements were quantified (Na, Mg, Al, Si, P, S, Cl, K, Ca, Ti, V, Cr, Mn, Fe, Ni, Cu, Zn, Br, Sr, Zr, Mo, Sn, Sb, Ba, Pb). Details of the methodology can be found elsewhere (Bukowiecki et al., 2005, 2008; Richard et al., 2010), with the following significant changes:

1. at SLS, we replaced the silicon drift detector (Roentec Xflash 2001 type 1102, Bruker AXS) with an e2v SiriusSD detector (SiriusSD-30133LE-IS). This detector is equipped with a thin polymer window resulting in a wider energy range down to about 300 eV and a better energy resolution of 133 eV (Mn Kα at 5.9 keV). In addition, the setup accepts a higher throughput resulting in negligible dead time effects. We also replaced the helium chamber with an in-house built vacuum chamber (sample exposure system for micro-X-ray fluorescence measurements, SESmiX) which reaches about 10^{-6} bar. This extended the measured range of elements down to Na and Mg.

2. Reference standards for calibration of element fluorescence counts to mass concentrations were produced on the same 6 μm PP substrate as used for RDI sampling, in contrast to the previous standard where a much thicker 25 μm PP foil was used. Two standards suitable for measurements at both SLS and HASYLAB contained elements in equal concentrations, and have a similar mix of elements as the standard previously used. Two additional standards containing only specifically selected light elements were produced. One standard contained Na, Al, P and Ca; the other Mg, Si, S, K and Ca. The concentrations of these elements were increased by a factor 3.8 relative to the other two standards to improve signal-to-noise ratios in the SR-XRF calibration. Co was added to these additional standards, but in the same concentration as in the other two foils and was used as

a quality check of the fabrication procedure of the four standards. The concentration difference of the light elements was taken into account before applying the relative calibration of the sample elements. The new reference standards allowed the use of identical geometry and irradiation time for RDI samples and reference standards, meaning that all SR-XRF measurements exhibit the same scattering and secondary fluorescence excitation. This reduced uncertainties in both the absolute and relative calibration of the samples.

3. Previously, spectra were fitted with the WinAxil software package (Canberra Inc; Van Espen et al., 1986). This rather old spectral fitting package allows little flexibility in spectrum continuum correction and peak fitting. PyMCA (Sole et al., 2007) on the other hand, is more flexible, but lacks the possibility to save uncertainty calculations in batch mode. In this study, spectra were fitted with an in-house developed software package called Spectral Analysis for Multiple Instruments – toolkit for XRF (SAMI-XRF) using the IGOR Pro software environment (Wavemetrics, Inc., Portland, OR, USA) to evaluate the data and create custom interfaces to accomplish specialized tasks. SAMI will be described in detail in a future manuscript. Briefly, SAMI sequentially determines (1) energy calibration of the X-ray line as a function of detector channel; (2) spectrum continuum correction; (3) peak width calibration as a function of energy (assuming Gaussian peak shape and a general square root law of the full-width-half-maximum (FWHM) energy relation); and (4) peak fitting of the entire spectrum, at which stage only peak heights are fitted as a free parameter and all other parameters are fixed. Steps (1) and (3) are performed with user-selected reference peaks, and incorporates fitting of complex (multi-Gaussian) peak shapes caused by nearly complete overlapping $K\alpha_1$ and $K\alpha_2$ lines. Step (2) utilizes collected spectra of a blank foil as a reference for the continuum shape, and scales this reference to user-selected element-free regions of the processed spectra. Step (4) allows lines to be fitted freely or fixed to another line, e.g. to the strongest line in a shell. For example, the $K\alpha_2$ and $K\beta$ lines are fixed to the $K\alpha_1$ line according to the relative intensities given by Bearden (1967).

Kerb and urban increment of trace elements in aerosol in London

S. Visser et al.

Title Page

Abstract	Introduction
Conclusions	References
Tables	Figures

|◄ | ►|

◄ | ►

Back | Close

Full Screen / Esc

Printer-friendly Version

Interactive Discussion

In this study, all lines within an electron shell were fitted fixed to the strongest line in that shell. Additionally, Ni, Cu and Zn $L\alpha_{1,2}$ lines were fixed to the $K\alpha_1$ line to reduce the influence of peak overlap with Na. The ratios of $L\alpha_{1,2}$ to $K\alpha_1$ for Ni, Cu and Zn were determined by fitting calibration standards having these elements but low Na. Final fits were then obtained using the acquired relations, thereby reducing uncertainties in the Na concentrations due to peak overlap and improving Na quantification.

2.2.2 Other measurements

Measurements from additional particle- and gas-phase instruments deployed at MR, NK and DE during the winter IOP discussed in this paper are described here. Daily PM_{10} filter samples (midnight to midnight) were collected at MR and NK using Partisol 2025 samplers (Thermo Scientific, Inc.). The filters were digested in a 1 : 2 mixture of perchloric and hydrofluoric acid, and subsequently analysed by inductively coupled plasma-mass spectrometry (ICP-MS) for the determination of Na, Al, Ca, Ti, V, Cr, Mn, Fe, Ni, Cu, Zn, Sr, Mo, Sb, Ba and Pb. Additionally, Mg, K and Sn were available at NK. High-resolution time-of-flight aerosol mass spectrometers (HR-ToF-AMS, Aerodyne Research, Inc., Billerica, MA, USA) were deployed with a 5 min resolution at MR, a 5 min resolution every 30 min at NK, and a 2 min resolution at DE to characterise the non-refractory submicron aerosol components (DeCarlo et al., 2006). PM_{10} mass concentrations were measured at all three sites with Filter Dynamics Measurement System Tapered Element Oscillating Microbalances (FDMS-TEOM; Thermo Scientific, Inc.) with a 1 h time resolution. NO_x measurements at MR and NK were performed with a NO_x chemiluminescent analyser with a single chamber and a single detector (API, A Series, model M200A) with a 15 min time resolution. At DE NO was collected with a Thermo Scientific 42i analyser and NO_2 with an Aerodyne CAPS-NO_2 (SN 1002) and an Aerodyne QCL-76-D. These NO and NO_2 measurements were summed together to obtain NO_x with a 1 min time resolution. Black carbon (BC) was measured with a 2-wavelength Aethalometer (λ = 370 and 880 nm, model AE22, Magee Scientific) at MR

and a 7-wavelength Aethalometer ($\lambda = 370$–$950\,nm$, model AE31, Magee Scientific) at NK and DE, all three with a time resolution of 5 min, and a $2.5\,\mu m$ cyclone at MR and DE and a $3.5\,\mu m$ cyclone at NK. Traffic counts by vehicle group at MR from road sensors (number of vehicles per 15 min) were available as well. Wind direction and wind speed data for MR and NK were taken from the BT Tower where anemometers were placed to the top of an open lattice scaffolding tower of 18 m height on top of the main structure (190.8 m a.g.l.; Wood et al., 2010), whereas local data were used at DE. Air mass origins were analysed with back trajectory simulations using the UK Met Office's Numerical Atmospheric Modelling Environment (NAME) dispersion model (Jones et al., 2007).

3 Data intercomparison

Previously, RDI-SR-XRF performance was analysed by Bukowiecki et al. (2005) and Richard et al. (2010). Both studies compared RDI-SR-XRF element concentrations with daily element concentrations from a high volume sampler with subsequent analysis by laboratory-based wavelength dispersive XRF (Bukowiecki et al., 2005) and by ICP-OES and ICP-MS (Richard et al., 2010). Most elements showed slopes between 0.7 and 1.6, except for S and K, with Pearson's $R > 0.5$. The spread/biases in these intercomparisons are not necessarily due to SR-XRF issues, as can be seen by a comparison by Salcedo et al. (2012) of ICP with proton-induced X-ray emission (PIXE) and AMS trace element measurements. Agreement between ICP and PIXE data was in the same range as between either method with the AMS with slopes ranging between 0.06 and 0.93 with Pearson's R from about 0.3 to 0.7. These studies show the challenges in the quantification of trace elements with different analysis techniques.

Here we compare RDI-SR-XRF data with independent filter data (24 h PM_{10} trace element data analysed with ICP-MS; roughly 9 % uncertainty at a 95 % confidence interval) for 19 elements collected at MR and NK (no filter data was available at DE). For this comparison, the three size ranges of the RDI were summed up to total PM_{10} and

averaged to the filter collection period. The intercomparison results are shown in Fig. 2, and are divided into four groups to facilitate discussion. Fit coefficients and Pearson's R values for the intercomparison are shown in Supplement Table S2. Elements shown in Fig. 2a (Al, Ca, Ti, Mn, Fe, Cu, Zn, Sr, Sb, Ba) agree within approximately ±50 %
5   with good correlations ($R > 0.74$). In Fig. 2b–d, we show elements for which the intercomparison shows significant biases and/or no significant correlation between RDI and filters. Note that the elements exhibiting good agreement in Fig. 2a span orders of magnitude difference in concentration (and fluorescence counts), suggesting that there are no global or concentration-dependent biases in the RDI-SR-XRF data. This
10 leaves the element relative calibration (i.e. element fluorescence yield as a function of line energy), spectral peak fitting, and instrument size cut points as issues to address.

Figure 2b shows good correlations for Mo ($R = 0.86$), but the RDI measures a factor 3 higher concentrations than found on the filters. Visual inspection of the spectrum indicates that significant interferences between lines are unlikely, and this is confirmed
15 by peak fitting sensitivity tests investigating the response of the calculated concentrations to uncertainties in line energy calibration (i.e. energy as a function of detector channel), the continuum, and calculated peak width. We estimate a 3 % uncertainty in the measurement of Mo due to spectral analysis. Strong correlations between filter and RDI time series also suggest that spectral fitting errors are not the cause of the
20 discrepancy. Mo falls in a well-constrained region of the calibration curve (although is not directly measured on calibration foils), so relative calibration errors would require a systematic bias across this entire region of the calibration curve. While there are not enough jointly measured elements within the intercomparison to evaluate this possibility, good agreement between RDI and filter measurements is obtained through Sr
25 ($K\alpha = 14.1$ keV) and at Sb ($K\alpha = 26.4$ keV) (Mo $K\alpha$ lines fall at 17.5 keV), suggesting such a bias is unlikely. For ICP-OES the extraction efficiency was unknown for Mo, potentially indicating that the filter data might be underestimated. The other elements (V, Cr, Ni) in Fig. 2b show no significant correlation between RDI and filters. Similar to the discussion of Mo, we do not expect significant spectral interferences for these

elements, and this is confirmed by the uncertainty analysis described above, which yielded around 20 % uncertainty for V, Cr and Ni. Unlike Mo, the relative calibration is well-constrained both in terms of elements directly measured on calibration foils and in terms of intercomparison with nearby elements in the XRF calibration curve, where V and Cr fall just above Ca and Ti and just below Mn and Fe, and Ni just above Mn and Fe and just below Cu and Zn. RDI and filter measurements are shown to be in good agreement for these six elements in Fig. 2a. However, the ICP-OES had an extraction efficiency for Ni of 66 %, whereas for V and Cr this was unknown, leading to increased uncertainties of these elements relative to others. Further, as shown in the following sections, the RDI time series of V, Cr and Ni (including both urban/kerb increments and diurnal/weekly cycles) are consistent with those of elements expected to be co-emitted by the same sources. We therefore assume the RDI V, Cr and Ni measurements to be valid, even though they are close to the minimum detection limits of SR-XRF.

Figure 2c shows good correlations for Na and Mg ($R > 0.87$), but the RDI concentrations are a factor 2 higher than the filters. The two measurement techniques each provide internally consistent results, with the Mg to Na ratio for the filter data at NK and the RDI data at NK and MR of approximately 0.13, which is close to the theoretical sea salt ratio of 0.12. The XRF relative calibration curve for Na and Mg is difficult to constrain due to the low response of these elements, but only led to an uncertainty of 10 %. The extraction efficiency for Mg in ICP-OES was 90 %, but was unknown for Na. However, it remains unclear why the results of both methods differ for these elements.

The elements K, Sn and Pb in Fig. 2d show reasonable to good correlations between RDI and filter measurements ($R > 0.53$) but the RDI data is only about half the filter data (filter measurements of K and Sn only at NK). Pb has a significant fraction of the mass in the fine fraction (see Fig. 3). Underestimation by the RDI is explained by an unexpectedly high small-end cut point of 290–410 nm (compared to 100 nm), as discussed below. K and Sn also have a significant fraction of their mass in the fine fraction, and might be affected by the cut off similarly to Pb.

Title Page

Abstract | Introduction

Conclusions | References

Tables | Figures

Back | Close

Full Screen / Esc

Printer-friendly Version

Interactive Discussion

S is a useful element for evaluation of the small-end cut off, as it is dominant in the fine fraction and measurable by several techniques. Therefore, we compared S data obtained with the RDI to simultaneous S mass calculated from sulphate (SO_4) measured by an AMS at MR, NK, and DE. The results in Supplement A show that the S mass in the RDI is on average about three times lower than that measured by the AMS. This is consistent with the discrepancy between RDI and filter measurements for fine fraction dominated elements. The RDI backup filter, which collects particles too small to impact at the $PM_{1.0-0.3}$ stage, was analysed for SO_4^{2-} using ion chromatography (Supplement A). Adding the S from this analysis to the S collected at the RDI $PM_{1.0-0.3}$ stage yielded mass closure with the S from AMS measurements within 20 % at all three sites. This suggests that elements with considerable mass in the small end of the $PM_{1.0}$ size range may be significantly underestimated. This affects S and Pb, and potentially also K, Zn, Br and Sn. To further investigate this underestimation, new RDI collection efficiency measurements for the $PM_{1.0}$ deposition stage were performed (Supplement A). The actual small-end cut off was determined to be 290–410 nm, rather than the previously measured value of 100 nm (Bukowiecki et al., 2009c; Richard et al., 2010), and found to be very sensitive to the machining tolerances of the $PM_{1.0}$ nozzle.

Only a small fraction of the measured elements are affected by this cut off issue. Further, because the analysis presented in the following sections depends on site-to-site ratios (for the same element) and relative concentration changes, potential biases are reduced by the similar (though not identical, see Supplement Fig. S2) cut offs of the different RDI units. The conclusions presented herein are thus not significantly affected by this artefact.

Kerb and urban increment of trace elements in aerosol in London

S. Visser et al.

Title Page

Abstract | Introduction

Conclusions | References

Tables | Figures

◄ | ►

◄ | ►

Back | Close

Full Screen / Esc

Printer-friendly Version

Interactive Discussion

4   Results and discussion

4.1   Trace element concentrations

During the ClearfLo winter IOP total mass concentrations of the analysed trace elements ranged from less than 0.01 to ~ 11 µg m^{-3}. Typically, concentrations were highest at MR and lower at NK and DE. Total trace element concentration in the coarse mode ranged on average from 0.8 to 3.7 µg m^{-3}. Intermediate mode concentrations ranged from 0.6 to 1.3 µg m^{-3}, whereas fine mode values varied between 0.5 and 0.6 µg m^{-3}. An overview of the obtained trace element concentrations as a function of size and site is given in Table 2. Note that S is not a trace element, but is commonly reported in trace element studies and is a good tracer for regional transport. Among the analysed trace elements, highest concentrations at MR were found for Na (26 %), Cl (23 %) and Fe (18 %), followed by Si (7 %), S (6 %) and Ca (5 %). At NK highest concentrations were found for Na (35 %), Cl (26 %) and Fe (9 %), followed by S (8 %), Mg (5 %) and Si (5 %). At DE highest concentrations were found for Na (35 %), Cl (24 %) and S (14 %), followed by Mg (6 %), Si (5 %) and Fe (4 %). Total analysed mass measured by the RDI-SR-XRF (trace elements + S) contributed on average 18 % to the total PM$_{10}$ mass (from FDMS-TEOM) of 32 (5–74) µg m^{-3} at MR (not extrapolated to the corresponding oxides), 14 % to the mass of 23 (1.4–63) µg m^{-3} at NK and 12 % to the mass of 17 (0.5–58) µg m^{-3} at DE.

A comparison between the contributions of coarse, intermediate and fine fractions to the total PM$_{10}$ mass of each trace element is shown in Fig. 3 for MR, NK and DE. The figure shows that MR trace elements are dominated by the coarse fraction. Analysis in the following sections and previous measurements at this site (Charron and Harrison, 2005) suggest this is caused by large contributions of resuspension and traffic-related mechanical abrasion processes, which primarily contribute to the coarse fraction. For all elements except S and Pb, the coarse fraction contributes more than 50 %. Mass fractions of intermediate mode elements to total PM$_{10}$ are rather constant with

contributions ranging from 14 to 28 %. The fine fraction contributes up to 50 % of total mass for S, K, Zn, Br and Pb; for other elements fine contributions are less than 17 %. S, K, Zn, Br and Pb are typically dominated by the fine fraction with known sources including heavy oil combustion (S, K, Zn; Lucarelli et al., 2000), traffic exhaust (Br, Pb; Formenti et al., 1996), industrial processes (Zn, Pb; Moffet et al., 2008), and secondary sulphate and wood combustion (S, K, Pb; Richard et al., 2011).

For most elements, particle mass contributions of the smaller size fractions are more important as one moves from kerbside to urban background to rural sites (Fig. 3). The large fine fraction contribution at DE is probably caused by the absence of local traffic which results in lower contributions of resuspension and traffic-related processes to total element concentrations, as discussed in the following sections. A different behaviour is observed for Cr and Mo with 80 % of their mass at DE in the coarse fraction, compared to 70 % at MR and 50 % at NK. The time series of coarse mode Cr and Mo are very spiky, correlate strongly with Ni, and are neither correlated to wind direction nor to wind speed, nor to collocated measurements of BC and AMS species, suggesting emissions from a local industrial source, potentially from stainless steel production (Querol et al., 2007; Witt et al., 2010) near DE rather than regional transport.

Comparing the contributions of groups of elements to total trace element concentrations at the sites provides an overview of local and regional sources affecting London; a detailed source apportionment study will be the subject of a future manuscript. Sea salt elements (Na, Mg, Cl) contribute around 60 % to the total PM_{10} trace element mass at all three sites, indicating that the air pollutant levels caused by elements are dominated by natural emission sources being transported to London. Note, however, that the absolute mass concentrations of these elements at MR are approximately 1.5 times higher than at NK and 2–3 times higher than at DE. This indicates the important role of anthropogenic activities (e.g. traffic) in the resuspension of these natural particles, but possibly also the application of road salt in winter (e.g. Lee et al., 1994). Mineral dust elements (Al, Si, Ca, Ti) mainly brought into the air via resuspension contribute 17 % to the total elemental mass at MR, 13 % at NK and 12 % at DE. For some

typical brake wear elements (Cu, Sb, Ba) these contributions are 1.4, 0.6 and 0.3 % at MR, NK and DE, respectively. Although these metals contribute a small fraction of total PM_{10} mass concentrations, they have adverse health effects. Xiao et al. (2013) e.g. found that Zn, Fe, Pb and Mn were the major elements responsible for plasmid DNA damage, whereas Kelly and Fussell (2012) found that increases in PM_{10} as a result of increased Ni, V, Zn and Cu contributions showed highest mortality risks, as opposed to increased Al and Si.

The RDI-SR-XRF technique is subject to various sources of uncertainty, which change in importance depending on whether the data are described in terms of absolute/fractional concentrations (as above) or in terms of relative changes/ratios (as in the remainder of the manuscript). A brief overview is presented here:

1. RDI sampling: the fluctuations in the flow rate are negligible within 5 % (Richard et al., 2010) and the uncertainties in the size cut off are discussed in Sect. 3.

2. SR-XRF accuracy: uncertainties in the absolute and relative calibrations affect absolute/fractional concentrations, but cancel out for relative changes/ratios, because all samples were measured under the same calibration conditions.

3. Issues such as imperfect flatness of the sample foils and detector dead time corrections (Richard et al., 2010) reduce measurement precision but affect all elements with the same scaling factor.

4. SR-XRF measurement precision is affected by sample inhomogeneity and spectral analysis uncertainties. Sample inhomogeneity was assessed by Bukowiecki et al. (2009c) and found to contribute ±20 % uncertainty. A comprehensive assessment of spectral analysis uncertainties is beyond the scope of the current work, but will be discussed in a future manuscript. The results of this analysis were discussed for selected elements in Sect. 3.

In addition, RDI-SR-XRF measurements (both absolute/fractional and relative/ratio) are affected by atmospheric variability. This variability is likely the predominant source of the data spread evident in Table 2 and the following analyses.

4.2 Urban and kerb increment

4.2.1 Urban increment

The urban increment compares the concentrations per trace element at the urban background site to the concentrations at the rural site, and is calculated here as the ratio of concentrations at NK to DE. Figure 4 shows the mean, median and 25–75th percentile urban increment ratios for coarse, intermediate and fine fractions per element. Most elements (except Cl, Ni, and coarse mode Cr and Mo) are enriched at the urban background site by factors between 1.0 and 4.7 (median ratios). The coarse and intermediate fractions show highest increment factors, while the fine fraction shows lower increments. Ni and coarse mode Cr show higher concentrations at DE relative to NK, as does the mean value of coarse Mo. As discussed in the previous section, enhanced coarse mode Cr, Ni and Mo may indicate a stainless steel production or other industrial source near DE. These elements show strong correlations with Pearson's R of ∼ 0.88 at DE vs. ∼ 0.57 at NK.

Coarse mode Zr exhibits low concentrations at DE, where the median value actually falls below detection limit, though discrete events above detection limit also exist. For this reason, the median-based urban increment is not plotted, while the mean ratio is driven by several large concentration peaks at NK, resulting in a large mean ratio of 9.5. In the case of Cl, a large spread in urban increment values is seen for all three size ranges. Cl is likely depleted relative to other sea salt elements like Na and Mg (throughout the campaign Cl concentrations fall to 0, where Na and Mg concentrations remain positive) due to replacement by nitrate, and the extent of such depletion is greater in small particles (Nolte et al., 2008). At DE, Cl depletion seems apparent at all size ranges, whereas at MR depletion only takes place in the $PM_{1.0-0.3}$ fraction.

NK shows Cl depletion especially in the $PM_{1.0-0.3}$ fraction, but to some extent also in intermediate mode particles.

Typical traffic related elements (Mn, Fe, Cu, Zn, Zr, Mo, Sn, Sb, Ba; see e.g. Amato et al., 2011; Bukowiecki et al., 2010; Minguillón et al., 2014; Richard et al., 2011; Viana et al., 2008) show urban increments on average of 3.0 in the coarse, 3.5 in the intermediate and 2.5 in the fine fraction (Fig. 4). These increments are similar to that of NO_x, where concentrations at NK were on average a factor 4.9 higher than at DE (mean concentration at NK was 68 ppb, at DE 14 ppb). However, black carbon (BC) had an urban increment of only 1.1 (concentration at NK 757 ng m^{-3}, at DE 633 ng m^{-3}), likely due to local wood burning emissions around DE (Mohr et al., 2013). Mineral dust elements (Al, Si, Ca, Ti, Sr; see e.g. Amato et al., 2009; Lin et al., 2005; Lucarelli et al., 2000) show a factor 2.3 higher concentrations at NK relative to DE in the coarse, 2.2 in the intermediate and 1.7 in the fine fraction. These results indicate that moving from rural to urban backgrounds yield a larger relative increase in traffic than in mineral dust elements. Surprisingly, sea salt elements (Na, Mg, Cl) show higher concentrations at NK than at DE of up to a factor of 2 for the coarse mode, despite the expected dominance of regional over local sources. This highlights the importance of sea or road salt resuspension by traffic. Similar urban increment values for traffic-related, resuspension and sea salt elements have been observed by Lee et al. (1994) for particles below a few µm. Theodosi et al. (2011) also found higher increments (> 2) for trace elements in PM_{10} aerosol from local anthropogenic sources like fossil fuel combustion (V, Ni, Cd) and traffic (Cu), relative to long range transported Saharan dust (Fe, Mn) with increments close to 1. However, our study suggests that the non-size-resolved values for increments reported in the cited studies do not fully capture the urban/rural differences.

The influence of regional transport in our study (Fig. 4) is seen by the urban increment between 1.2 and 2.0 for P, S, K, Zn, Br and Pb in $PM_{1.0-0.3}$ and of 1.6 for total PM_{10} mass (concentration at NK 23 µg m^{-3}, at DE 17 µg m^{-3}). The concentrations of the main components in PM_{10} (sulphate, nitrate and secondary organic compounds) within an urban area are mostly influenced by regional transport, as found in London during the

Title Page

Abstract | Introduction

Conclusions | References

Tables | Figures

|◄ | ►|

◄ | ►

Back | Close

Full Screen / Esc

Printer-friendly Version

Interactive Discussion

REPARTEE project (Harrison et al., 2012a) and in Paris during the MEGAPOLI project (Crippa et al., 2013; Freutel et al., 2013), resulting in low increments for total PM$_{10}$ mass. Similar urban increment values (1.3 to 1.8) for 1 and 24 h total PM$_{2.5}$ mass concentrations were reported across many sites in the UK (Harrison et al., 2012c).

4.2.2 Kerb increment

While the urban increment investigates the effect of diffuse emission sources on particle concentrations, the kerb increment investigates an urban micro-environment, specifically the local effects of roadside emissions and activities. Here, the kerb increment is calculated as the ratio of concentrations at MR to NK. However, observed concentrations strongly depend on wind direction, because the road runs from approximately 260° to 80° and the street canyon with the surrounding buildings and intersections creates a complex wind circulation system (Balogun et al., 2010). The influence of wind direction on the air pollutant concentrations in the street canyon at MR was identified by e.g. Balogun et al. (2010), Charron and Harrison (2005) and Harrison et al. (2012b), with higher concentrations corresponding with SSE winds, i.e. perpendicular to the direction of the road. Since the measurement station is located at the southern side of the canyon, measurements during time periods with winds from the south are influenced by on-road emissions on top of the urban background pollution.

In this study we have averaged the 30 min wind direction data collected at the elevated BT Tower to the RDI 2 h time resolution at MR and NK, and the 1 min wind direction data collected at DE to the RDI 2 h time resolution at the same site. The RDI-SR-XRF data was split into four equally spaced wind direction sectors; N (315–45°), E (45–135°), S (135–225°) and W (225–315°). Figure 5 shows size-resolved trace element concentrations per wind sector normalized to the global median concentration for each element at MR. Winds from the south yield the highest concentrations, whereas northern winds yield the lowest, independent of size fraction. West and east winds are parallel to the street canyon and yield intermediate concentrations, consistent with e.g. Charron and Harrison (2005) and Harrison and Jones (2005). Similar behaviour is

observed for NO_x, and no directional biases for high wind speeds are observed (Supplement Fig. S5).

Figure 5 shows that typical traffic-related elements from exhaust emissions and brake and tire wear (V, Cr, Mn, Fe, Ni, Cu, Zn, Zr, Mo, Sn, Sb, Ba) are about a factor 3 higher during S compared to N winds for the coarse fraction, and a factor of 2 for the intermediate and fine fractions. Although some studies have assigned V and Ni to industrial sources (Mazzei et al., 2007) and Zr to soil-related particles (Moreno et al., 2013), here they are empirically grouped with traffic elements due to their similar kerb increments and diurnal/weekly cycles (Sect. 4.3). This does not rule out effects from other sources (e.g. industrial influences on Ni can be observed at the low-traffic rural site), but suggest that traffic is the dominant emission source at the kerbside site. The attribution of e.g. Zr to traffic is consistent with previous studies (Amato et al., 2011; Bukowiecki et al., 2009b, 2010).

Resuspended mineral dust elements (Al, Si, Ca, Ti, Sr) show smaller enrichments than elements related to wearing and exhaust emissions, with concentration ratios for S to N wind conditions of approximately 2 for the coarse fraction, and 1.5 for intermediate and fine fractions. Harrison et al. (2012b) found a ratio of 2 for Fe (as tracer for brake wear) and 1.2 for Al (as tracer for mineral dust) for SW vs. NE winds for particles between 2 and 3 µm. However, they were limited by their time resolution of several days, needed to sample enough PM to be quantitative, which resulted in potentially substantial wind direction variations during each measurement and possibly in reduced ratios.

In the coarse and intermediate mode, Na, Mg, S, Cl, K and Br show only minor correlations with wind direction (Fig. 5), indicating that these elements are influenced more by regional transport, instead of being locally emitted by traffic. In the fine mode, Na and Mg also show little wind direction influence, whereas S, K and Br seem to be enriched with winds from the east, potentially related to long-range transport from the European continent. Cl is highly variable in all four wind sectors, and, as discussed previously, is likely depleted throughout the campaign by nitrate chemistry.

Title Page

Abstract | Introduction

Conclusions | References

Tables | Figures

|◄ | ►|

◄ | ►

Back | Close

Full Screen / Esc

Printer-friendly Version

Interactive Discussion

Local wind direction has a greatly reduced effect at urban background and rural sites. At NK, the element concentrations are less influenced by wind direction (Fig. S3 of the Supplement), but subject to high concentration outliers for E winds. This could be caused by the transport of pollutants from emission sources in downtown London, or by
5 lower wind speeds occurring with E winds resulting in reduced dilution and increased concentrations of traffic pollutants (e.g. NO_x) throughout the city (Supplement Fig. S5). The rural site also shows a slight wind direction dependency (Supplement Fig. S4). Here, winds from N and E sectors result in enhanced concentrations relative to S and W sectors, especially in the fine mode. Interpretation of data from the E sector is unclear
10 due to the low number of data points (45 out of 323 data points). These wind directions were accompanied by low wind speeds (Fig. S5 of the Supplement), reducing dilution and leading to the accumulation of pollutants emitted from villages and towns in the surrounding area (Mohr et al., 2013). Data from the N sector correspond to higher wind speeds and back trajectories consistent with transport from continental Europe.
15 To simplify reporting of the kerb increment and facilitate comparison with previous studies (e.g. Harrison et al., 2012b), we combined the south/west sectors and the north/east sectors into SW (135–315°) and NE (315–135°) sectors. To eliminate meteorological and/or regional transport effects, this segregation is performed at both MR and NK. The kerb increment is then calculated as the ratio of MR to NK and shown in Fig. 6
20 (Supplement Fig. S6 shows the increment for the 4 individual sectors). As with the urban increment, we focus on the ratio of the medians at MR and NK to reduce the effects of outliers. Two features become directly visible; the kerb increment is much higher for coarse than for intermediate and fine particles, and kerb increments are much higher for SW than for NE wind conditions. Even for NE conditions, kerb increments are on
25 average 3.3 for coarse, 1.5 for intermediate and 1.4 for fine mode particles. This significant enhancement is likely due to recirculation of particles within the street canyon following their resuspension and/or emission by traffic. However, these increments are much smaller than those observed in the SW sector, where enhancements relative to NK of 7.2 for coarse, 3.4 for intermediate and 2.7 for fine mode elements are observed.

Discussion Paper | Discussion Paper | Discussion Paper | Discussion Paper

These results indicate the existence of micro-environments within the street canyon dependent on wind direction.

Several elements can be grouped according to their similarity in kerb increments (Fig. 6). The first group consists of Cu, Zr, Mo, Sn, Sb and Ba and yields the highest increments in the coarse mode ranging from 11.6 to 18.5 in the SW sector (3.6–9.4 for NE). These elements are typically associated with brake wear (e.g. Bukowiecki et al., 2009b; Harrison et al., 2012b), and are much higher than the increments of 4.1 to 4.4 reported by Harrison et al. (2012b) at the same sites for particles $< 21\,\mu m$ (Fe, Cu, Sb and Ba were assigned to brake wear). However, when combining all size fractions and ignoring wind direction influences, increments in this study are about 5.1, and more similar to previous studies. The discrepancies between the kerb increments obtained using these two calculation strategies highlights the difficulties in characterizing human exposure to locally generated pollutants in urban environments, as the detailed topography and microscale meteorology greatly alter particle concentrations, and the effects are size-dependent. Amato et al. (2011) calculated road side increments in Barcelona for trace elements in PM_{10} with a 1 h time resolution and found increments for brake wear elements of 1.7 (Fe, Cu, Sb, Cr, Sn as tracers for brake wear). These low increments are probably due to the reduced dispersion in Barcelona caused by a complex topography, resulting in high urban background levels.

The second group consists of elements that might be affected by other traffic-related processes than brake wear (V, Cr, Mn, Fe, Ni, Zn, Pb) with increments of 5.6 to 8.0 in the SW sector (2.6–6.5 for NE) (Fig. 6). Zn is usually associated with tire wear (e.g. Harrison et al., 2012b; Lin et al., 2005), and the other elements are commonly associated with traffic-related emissions (e.g. Amato et al., 2013; Bukowiecki et al., 2009a; Richard et al., 2011). These increments are similar to the ones for NO_x of 8.5 for SW and 2.4 for NE, confirming the influence of traffic on these elements. The high braking frequency at MR due to congested traffic probably resulted in increased kerb increments of brake wear relative to other traffic-related elements that are also emitted by local traffic at NK. Similar to the brake wear elements, combining all size fractions and

ignoring wind direction influences yield kerb increments of about 3.1 (4.8, 2.3 and 2.1 for coarse, intermediate and fine mode, respectively), which mask the systematically higher values recorded for specific locations/meteorological conditions in the micro-environment. These averaged values are however similar to the 2.8 for PM_{10} trace elements (time resolution of 42 h per week) reported in the Netherlands (Boogaard et al., 2011), and to the 4.5 and 3.2 for Fe in PM_{10} and $PM_{2.5}$, respectively (daily measurements) also found in the Netherlands (Janssen et al., 1997). However, reported increments for V, Mn and Zn are below 1.8 and much smaller than found at MR relative to NK. The high increments presented here might be caused by street canyon effects, trapping pollutants emitted at street level and preventing dilution to the urban background. In more open street sites pollutants are diluted more easily, resulting in reduced concentration differences between street and urban background sites. The enhanced kerb increments for brake wear relative to other traffic-related elements is apparent in all three size fractions, although increments become more similar towards smaller sizes with a factor 1.9 between both element groups in the coarse, 1.5 in the intermediate and 1.2 in the fine mode. Both traffic-related groups show the additional information gained with size-segregated aerosol, where exposure to trace elements in the street canyon relative to the urban background increases with particle size, either caused by increased traffic-related emissions with particle size or by more efficient transport of submicron particles from street sites to the urban background. Furthermore, the highly time-resolved element measurements presented here enabled us to resolve the systematic, wind direction dependent variability in the kerb increment.

The third group is associated with mineral dust (Al, Si, Ca, Ti, Sr) and coarse mode kerb increments for the SW sector yield 3.3 to 5.2 (1.8–2.4 for NE) (Fig. 6). These elements are brought into the air both by traffic-induced resuspension and transport from other locations. This second process increases both urban background and kerb-side concentrations, and thus reduces kerb increments relative to direct traffic-related elements. Lower kerb increments for mineral dust than traffic-related elements are generally observed in kerb increment studies (Amato et al., 2011; Boogaard et al., 2011;

Bukowiecki et al., 2009b; Harrison et al., 2012b), although the dust increments found in this study are larger than most reported increments (typically between 1 and 2). As in the traffic-related groups, increments increase with particle size, indicating that human exposure at the street side is enhanced for particles above 1 µm.

Sea salt (Na, Mg, Cl) forms the fourth group and yields kerb increments of 1.0 to 2.0, independent of size fraction but with slightly enhanced ratios with SW compared to NE winds (Fig. 6). Similar increments were observed for total PM_{10} mass. As discussed for urban increments, even though these elements have regional sources, they are influenced by resuspension processes within the urban area which are enhanced at kerbside sites.

The remaining elements (P, S, K, Br) can be grouped together. In the coarse mode, these elements yield increments similar to the mineral dust group, indicating that this group is influenced by resuspension processes in the street canyon (Fig. 6). However, especially in the fine mode increments around 1 were found, consistent with regional transport dominating over local emission sources.

4.3 Temporal trends in trace element concentrations

In contrast to traditional trace element measurements, the RDI-SR-XRF enables measurement of element concentrations with high time resolution (2 h in this work). This enables investigation of diurnal cycles, which are useful both for source discrimination and in determining the processes contributing to elevated PM levels. We also discuss weekly cycles, which can be useful in distinguishing emissions from heavy duty and passenger vehicles; heavy duty vehicle numbers typically diminish during the weekend. Back trajectory analysis aids source discrimination by understanding regional transport influences by different air mass origin. Here we discuss the temporal trends of trace elements in five groups based on expected sources and the increment analyses in the Sect. 4.2, in order of increasing local influence: regional background, sea salt, mineral dust, traffic-related and brake wear.

Figures 7 and 8 show size-segregated median diurnal and weekly cycles, respectively, for 5 elements representative of the classes mentioned above: Na (sea salt), Si (mineral dust), S (regional background), Fe (traffic-related) and Sb (brake wear) at MR, NK and DE. Because of the wind direction effect evident at MR, diurnal cycles at all three sites are shown for SW and NE winds. Wind direction analyses are not incorporated into the weekly cycles because the month-long campaign provided insufficient data points for meaningful division. This also means that weekly cycles are subject to influences by mesoscale events. For example, sea salt shows no clear weekly cycle, except for a peak on Fridays in intermediate and fine fractions coinciding with westerly winds, which coincidentally occurred more frequently on Fridays than on other days. Except for such events, regionally dominated elements tend to display flat, featureless diurnal/weekly cycles, while elements dominated by recurring local processes (e.g. traffic patterns) show interpretable features. Diurnal and weekly cycles of all other elements can be found in Supplement Figs. S7 and S8. For comparison, diurnal and weekly cycles of NO_x and total PM_{10} mass at all sites, and of traffic flow at MR are shown in Fig. 9. The time series of these species were averaged to the RDI collection times before obtaining the cycles. BC diurnal and weekly cycles (not shown) are very similar to those of NO_x.

4.3.1 Regional influences

Elements dominated by regional sources (P, S, K, Br) occur mainly in the fine fraction and are similar to total PM_{10} mass in showing no obvious diurnal and weekly patterns. This interpretation is consistent with the urban/kerb increment analysis discussed in Sect. 4.2. Weekly patterns suggest fine Zn and Pb are also dominated by regional transport (Supplement Fig. S8). P, S and K have been identified as tracers for mixed wood combustion and secondary sulphate (Amato et al., 2011; Richard et al., 2011), whereas Hammond et al. (2008) have identified S, K and Pb from mixed secondary sulphate and coal combustion. Br is usually associated with sea salt (Lee et al., 1994; Mazzei et al., 2007) or traffic emissions (Gotschi et al., 2005; Lee et al., 1994), but

Maenhaut (1996) has also found Br, together with S, K, Pb and other elements in biomass burning. In this study, the diurnal cycle of fine Br is different from the Na, Mg and Cl cycles, and is more similar to K. Br is thus more likely associated with wood burning than with other sources.

The time series of this group of elements (fine S, K, Zn, Pb) at NK is explored in relation to total PM_{10} mass, wind direction at the BT Tower and air mass origin, and compared to representative elements from the other emission groups (coarse Na, Si, S, Sb; Fig. 10). Air mass origin was studied with back trajectories simulated for three case study periods (marine, European mainland and locally influenced) using the NAME model (Jones et al., 2007). Particles are released into the model atmosphere from the measurement location and their origin is tracked using meteorological fields from the Unified Model, a numerical weather prediction model. Each particle carries mass of one or more pollutant species and evolves by various physical and chemical processes during 24 h preceding arrival at NK. Potential emission source regions can be high-lighted along the pathway to the measurement site at 0–100 m above ground. The time series of these fine mode elements at MR and DE (not shown) are very similar to NK, consistent with the absence of an increment and thus the predominance of regional sources for these elements.

Case A in Fig. 10 is at the end of a period with predominantly westerly winds (18–24 January) and a marine air mass origin associated with high wind speeds (air has travelled a long distance in 24 h). Although the air mass has also passed over Ireland and the Midlands, the influence of these rather sparsely populated regions on pollu-tion levels is small. Under these conditions concentrations of fine S, K, Zn and Pb are fairly low. In comparison, sea salt elements (see coarse Na in Fig. 10) are enhanced during this period. Total PM_{10} mass and NO_x (not shown) concentrations are low as well, showing that with strong westerlies pollution levels at NK are low and not strongly influenced by traffic. In case B (right in the middle of a 3 day episode), north easterlies (with high wind speeds) from the European continent bring in pollutants through re-gional transport leading to a large regional pollution episode characterised by elevated

concentrations of fine S, K, Zn and Pb. Total PM_{10} mass showed strongly enhanced concentrations as well. During this episode, both the urban background and rural site observed the highest concentrations for these trace elements of the entire campaign. However, mineral dust and traffic-related elements, as well as NO_x, were not enhanced at the urban background in case B. Wind direction in case C is variable, but the NAME footprint shows local air mass stagnation over London and the southeast of the UK accompanied by low wind speeds. This local pollution episode of roughly 3 days resulted in elevated concentrations of all trace elements, NO_x and total PM_{10} mass (NK no data, MR and DE elevated concentrations), independent of emission source. The very high concentrations observed in case B through regional transport from the European mainland were identified as the main reason for PM_{10} limit exceedances at urban background sites in London by Charron et al. (2007), while exceedances were much less frequent under marine influenced air as represented by case A in this study.

4.3.2 Sea salt

The sea salt group (Na, Mg, Cl) yields comparable, rather flat diurnal cycles for fine and intermediate mode Na, Mg and Cl, and coarse mode Na and Cl (Na in Fig. 7; others in Fig. S7 of the Supplement), and no obvious weekly patterns (Na in Fig. 8; others in Supplement Fig. S8). This indicates that the regional transport of sea salt is probably the main source of Na, Mg and Cl, as seen in case A in Fig. 10.

Interestingly, although coarse mode sea salt exhibits no obvious temporal trend, the urban and kerb increment indicates additional source contributions besides regional transported sea salt. The urban increment might be caused by the natural sea salt gradient observed in the UK, with reducing concentrations from west to east (Fowler and Smith, 2000), while the kerb increment could be the result of road salt resuspension in addition to sea salt resuspension. The effects of road salt are supported by enhanced kerb increments (~ 2.0) with respect to the ClearfLo summer IOP (~ 1.4; not published). Coarse mode Mg originates probably both from mineral dust and sea salt,

because at MR with SW winds Mg correlates with Al and Si temporal trends, while with NE winds Mg correlates better with Na and Cl.

4.3.3 Mineral dust and traffic

Both mineral dust and traffic-related elements are strongly influenced by traffic patterns at MR, which are shown in Fig. 9 as the number of vehicles per 2 h split in light (passenger) and heavy duty vehicles (shorter/longer than 5.2 m). Heavy duty vehicle numbers peak in the morning, whereas passenger vehicle numbers peak in the evening when the flow of traffic leaves the urban area, consistent with Harrison et al. (2012b). A single peak during midday in the weekend compared to a double peak at weekdays is observed for light duty vehicles. Heavy duty vehicle numbers show a similar pattern during weekdays (morning maximum), a reduced maximum on Saturday and a small maximum that is shifted towards midday on Sunday. Charron and Harrison (2005) reported similar traffic patterns during two years of traffic counts, and stated very small week-to-week variability, except during holidays.

The element diurnal (Fig. 7 for Si, Fe and Sb; Supplement Fig. S7 for others) and weekly (Fig. 8 for Si, Fe and Sb; Supplement Fig. S8 for others) cycles yield highest concentrations at MR and lower concentrations at NK and DE, consistent with observed urban and kerb increments. Concentrations are higher during the day than at night, with night time concentrations at MR and NK similar to median urban background and rural concentrations, respectively, demonstrating the effects of local traffic. Weekdays yield stronger increments than weekends and closely follow NO_x and heavy duty vehicle traffic patterns (Fig. 9), indicating the strong influence of these vehicles on element concentrations. This is consistent with observations by Charron et al. (2007), who observed that PM_{10} limit exceedances at MR are more likely to occur on weekdays, in combination with large regional contributions from the European mainland with easterly winds. Similarly, Barmpadimos et al. (2011) found strong weekly cycles for $PM_{10-2.5}$ and $PM_{2.5}$ mass concentrations in Switzerland over a 7–12 year period, with higher concentrations on weekdays and lowest on Sundays.

Title Page

Abstract | Introduction

Conclusions | References

Tables | Figures

◄ | ►

◄ | ►

Back | Close

Full Screen / Esc

Printer-friendly Version

Interactive Discussion

At MR with SW winds, all coarse mode elements except Na and Cl exhibit a double peak in the diurnal cycles, closely following the flow of traffic and confirming that element concentrations in the street canyon are mainly driven by traffic instead of mesoscale meteorological processes (see Charron et al., 2007). Especially during rush hour, most braking and stationary queues occur due to the heavily used pedestrian traffic light-controlled crossing and the signal-controlled junction in close proximity to the measurement site, leading to enhanced concentrations of brake wear elements and possibly also to increased resuspension, especially induced by heavy duty vehicles (Bukowiecki et al., 2009a). With NE winds, source discrimination based on diurnal patterns is possible between mineral dust (e.g. Si in Fig. 7) and traffic-related elements (e.g. Fe and Sb in Fig. 7). Mineral dust yields a strong maximum between 08:00 and 14:00 LT, and continued high concentrations throughout the day, while the traffic-related group yields a reduced double peak relative to SW winds. The increase in mineral dust concentrations coincides with the start of traffic flows at 06:00 LT resulting in resuspension of particles within the street canyon. However, concentrations decrease before traffic flows reduce, possibly as a result of increased mixing during the day with growth of the mixing layer. At NK diurnal and weekly patterns for mineral dust and traffic-related elements yield similar variability but reduced concentrations relative to MR, which suggests increased human exposure during day time and weekdays and confirms that traffic dominates urban background element concentrations in London (see Dore et al., 2003). At DE, freshly emitted pollutants from London and other cities in the south eastern UK have been diluted and mixed with other pollutants during their transport to the rural background, resulting in no obvious diurnal and weekly patterns independent of size range.

The kerb increments at MR under SW winds were divided into two traffic-related groups: brake wear (Cu, Zr, Mo, Sn, Sb, Ba) and other traffic-related (V, Cr, Mn, Fe, Ni, Zn, Pb) elements. However, the diurnal and weekly cycles of all these elements correlate well and no obvious split into two groups is seen. Apparently, both groups are co-emitted as a single group under comparable vehicle fleet and/or set of driving

conditions, at least on a 2 h time scale, but in different ratios at MR and NK. The ratio of these two element classes for SW to NE wind sectors at MR is about 2.5, with the lack of difference between these classes supporting co-emission. In a future manuscript we will further explore the diurnal variability of emission sources at both sites with statistical analyses based on the multilinear engine (Canonaco et al., 2013; Paatero, 1999).

5 Conclusions

Aerosol trace element composition was measured at kerbside, urban background and rural sites in the European megacity of London during winter 2012. Sampling with rotating drum impactors (RDI) and subsequent measurements with synchrotron radiation-induced X-ray fluorescence spectrometry (SR-XRF) yielded trace element mass concentrations in $PM_{10-2.5}$, $PM_{2.5-1.0}$ and $PM_{1.0-0.3}$ aerosol with a 2 h time resolution. Total median element mass of 4.6, 2.4 and 1.0 $\mu g\,m^{-3}$ were found at kerbside, urban background and rural sites, respectively, which constitutes 12 to 18 % to total PM_{10} mass (highest at kerbside; lowest at rural site), neglecting the corresponding oxides. The contribution of emission sources to coarse fraction elements was on average largest at kerbside (63 %) and reduced for urban background (47 %) and rural sites (44 %).

Urban and kerb increments were defined as the concentration ratios of urban background to rural, and kerbside to urban background, respectively, and the kerb increments were further explored as a function of wind direction. Traffic-related elements (Mn, Fe, Cu, Zn, Zr, Mo, Sn, Sb, Ba) yielded largest kerb and urban increments, with kerb increment values ranging between 5.8 and 18.5 for SW winds (2.6–9.4 for NE winds) and urban increments of around 3.0. Traffic-related kerb increments could be further divided into elements from brake wear and other traffic-related processes. Brake wear elements (Cu, Zr, Mo, Sn, Sb, Ba) showed a factor 2 larger increments than other traffic-related elements (11.6–18.5 vs. 5.6–8.0 in coarse mode with SW winds). Kerb increments for these traffic-related elements in the $PM_{10-2.5}$ size fraction are roughly 3 times that of the $PM_{1.0-0.3}$ fraction, and are also highest for SW winds due to local street

Back | Close

Full Screen / Esc

Printer-friendly Version

Interactive Discussion

canyon effects. In addition to direct emissions, traffic-related processes influence the concentrations of other elements by resuspension, with mineral dust increments (Al, Si, Ca, Ti, Sr) of 1.7–4.1. Diurnal cycles of mineral dust elements and coarse Na, Mg and Cl both indicate major concentration enhancements during periods of heavy traffic, whereas regionally-influenced elements ($PM_{1.0-0.3}$ P, S, K, Zn, Br, Pb) showed no enhancements. All traffic-related elements at the kerbside site yielded temporal patterns similar to variations in heavy duty vehicle numbers as opposed to total vehicle numbers, and resulted in enhanced exposure to elements during day time and weekdays. Traffic-related processes therefore exhibit a dominant influence on air quality at the kerbside and urban background sites, and should be the main focus of health effect studies and mitigation strategies. With technological improvements for the reduction of traffic exhaust emissions, the traffic contribution to coarse PM is becoming more important as shown by decreasing $PM_{2.5}$ mass trends with no significant changes of coarse PM (Barmpadimos et al., 2012).

Trace element and total PM_{10} mass concentrations are also affected by mesoscale meteorology, increasing with the transport of air masses from the European mainland. Under these conditions, coarse and intermediate fraction trace elements are hardly affected, but fine fraction elements (P, S, K, Zn, Br, Pb) showed elevated concentrations. Trace element concentrations in London are therefore influenced by both local and regional sources, with coarse and intermediate fractions dominated by anthropogenic activities (particularly traffic-induced resuspension and wearing processes), whereas fine fractions are significantly influenced by regional processes.

These observations highlight both the strong influence of regional factors on overall air quality, as well as the need for detailed characterization of urban microenvironments for accurate assessment of human exposure to airborne particulates and the associated health risks.

The Supplement related to this article is available online at doi:10.5194/acpd-14-15895-2014-supplement.

References

15 Amato, F., Pandolfi, M., Escrig, A., Querol, X., Alastuey, A., Pey, J., Perez, N., and Hopke, P. K.: Quantifying road dust resuspension in urban environment by Multilinear Engine: a comparison with PMF2, Atmos. Environ., 43, 2770–2780, 2009.

Amato, F., Viana, M., Richard, A., Furger, M., Prévôt, A. S. H., Nava, S., Lucarelli, F., Bukowiecki, N., Alastuey, A., Reche, C., Moreno, T., Pandolfi, M., Pey, J., and Querol, X.:
20 Size and time-resolved roadside enrichment of atmospheric particulate pollutants, Atmos. Chem. Phys., 11, 2917–2931, doi:10.5194/acp-11-2917-2011, 2011.

Amato, F., Schaap, M., Denier van der Gon, H. A. C., Pandolfi, M., Alastuey, A., Keuken, M., and Querol, X.: Short-term variability of mineral dust, metals and carbon emission from road dust resuspension, Atmos. Environ., 74, 134–140, 2013.

25 Arnold, S. J., ApSimon, H., Barlow, J., Belcher, S., Bell, M., Boddy, J. W., Britter, R., Cheng, H., Clark, R., Colvile, R. N., Dimitroulopoulou, S., Dobre, A., Greally, B., Kaur, S., Knights, A., Lawton, T., Makepeace, A., Martin, D., Neophytou, M., Neville, S., Nieuwenhuijsen, M., Nickless, G., Price, C., Robins, A., Shallcross, D., Simmonds, P., Smalley, R. J., Tate, J., Tomlin, A. S., Wang, H., and Walsh, P.: Introduction to the DAPPLE air pollution project, Sci. Total
30 Environ., 332, 139–153, 2004.

Balogun, A. A., Tomlin, A. S., Wood, C. R., Barlow, J. F., Belcher, S. E., Smalley, R. J., Lingard, J. J. N., Arnold, S. J., Dobre, A., Robins, A. G., Martin, D., and Shallcross, D. E.: In-street wind direction variability in the vicinity of a busy intersection in central London, Bound.-Lay. Meteorol., 136, 489–513, doi:10.1007/s10546-010-9515-y, 2010.

5 Barmpadimos, I., Nufer, M., Oderbolz, D. C., Keller, J., Aksoyoglu, S., Hueglin, C., Baltensperger, U., and Prévôt, A. S. H.: The weekly cycle of ambient concentrations and traffic emissions of coarse (PM_{10}–$PM_{2.5}$) atmospheric particles, Atmos. Environ., 45, 4580–4590, 2011.

Barmpadimos, I., Keller, J., Oderbolz, D., Hueglin, C., and Prévôt, A. S. H.: One decade of

10 parallel fine ($PM_{2.5}$) and coarse (PM_{10}–$PM_{2.5}$) particulate matter measurements in Europe: trends and variability, Atmos. Chem. Phys., 12, 3189–3203, doi:10.5194/acp-12-3189-2012, 2012.

Bearden, J. A.: X-ray wavelengths, Rev. Mod. Phys., 39, 78–124, doi:10.1103/RevModPhys.39.78, 1967.

15 Bigi, A. and Harrison, R. M.: Analysis of the air pollution climate at a central urban background site, Atmos. Environ., 44, 2004–2012, 2010.

Bohnenstengel, S. I., Evans, S., Clark, P. A., and Belcher, S. E.: Simulations of the London urban heat island, Q. J. Roy. Meteor. Soc., 137, 1625–1640, doi:10.1002/qj.855, 2011.

Bohnenstengel, S. I., Belcher, S. E., Allan, J. D., Allen, G., Bacak, A., Bannan, T. J., Barlow, J. F.,

20 Beddows, D. C. S., Bloss, W. J., Booth, A. M., Chemel, C., Coceal, O., Di Marco, C. F., Faloon, K. H., Fleming, Z., Furger, M., Geitl, J. K., Graves, R. R., Green, D. C., Grimmond, C. S. B., Halios, C., Hamilton, J. F., Harrison, R. M., Heal, M. R., Heard, D. E., Helfter, C., Herndon, S. C., Holmes, R. E., Hopkins, J. R., Jones, A. M., Kelly, F. J., Kotthaus, S., Langford, B., Lee, J. D., Leigh, R. J., Lewis, A. C., Lidster, R. T., Lopez-Hilfiker, F. D.,

25 McQuaid, J. B., Mohr, C., Monks, P. S., Nemitz, E., Ng, N. L., Percival, C. J., Prévôt, A. S. H., Ricketts, H. M. A., Sokhi, R., Stone, D., Thornton, J. A., Tremper, A. H., Valach, A. C., Visser, S., Whalley, L. K., Williams, L. R., Xu, L., Young, D. E., and Zotter, P.: Meteorology, air quality and health in London: the ClearfLo project, B. Am. Meteorol. Soc., in review, 2013a.

30 Bohnenstengel, S. I., Hamilton, I., Davies, M., and Belcher, S. E.: Impact of anthropogenic heat emissions on London's temperatures, Q. J. Roy. Meteor. Soc., 140, 687–698, doi:10.1002/qj.2144, 2013b.

Boogaard, H., Kos, G. P. A., Weijers, E. P., Janssen, N. A. H., Fischer, P. H., van der Zee, S. C., de Hartog, J. J., and Hoek, G.: Contrast in air pollution components between major streets and background locations: particulate matter mass, black carbon, elemental composition, nitrogen oxide and ultrafine particle number, Atmos. Environ., 45, 650–658, 2011.

Bukowiecki, N., Hill, M., Gehrig, R., Zwicky, C. N., Lienemann, P., Hegedus, F., Falkenberg, G., Weingartner, E., and Baltensperger, U.: Trace metals in ambient air: hourly size-segregated mass concentrations determined by synchrotron-XRF, Environ. Sci. Technol., 39, 5754–5762, 2005.

Bukowiecki, N., Lienemann, P., Zwicky, C. N., Furger, M., Richard, A., Falkenberg, G., Rickers, K., Grolimund, D., Borca, C., Hill, M., Gehrig, R., and Baltensperger, U.: X-ray fluorescence spectrometry for high throughput analysis of atmospheric aerosol samples: the benefits of synchrotron X-rays, Spectrochim. Acta B, 63, 929–938, 2008.

Bukowiecki, N., Gehrig, R., Lienemann, P., Hill, M., Figi, R., Buchmann, B., Furger, M., Richard, A., Mohr, C., Weimer, S., Prevot, A. S. H., and Baltensperger, U.: PM_{10} Emission Factors of Abrasion Particles From Road Traffic, Schweizerische Eidgenossenschaft, UVEK/ASTRA, Report 1268, 195 pp., 2009a.

Bukowiecki, N., Lienemann, P., Hill, M., Figi, R., Richard, A., Furger, M., Rickers, K., Falkenberg, G., Zhao, Y. J., Cliff, S. S., Prevot, A. S. H., Baltensperger, U., Buchmann, B., and Gehrig, R.: Real-world emission factors for antimony and other brake wear related trace elements: size-segregated values for light and heavy duty vehicles, Environ. Sci. Technol., 43, 8072–8078, 2009b.

Bukowiecki, N., Richard, A., Furger, M., Weingartner, E., Aguirre, M., Huthwelker, T., Lienemann, P., Gehrig, R., and Baltensperger, U.: Deposition uniformity and particle size distribution of ambient aerosol collected with a rotating drum impactor, Aerosol Sci. Tech., 43, 891–901, 2009c.

Bukowiecki, N., Lienemann, P., Hill, M., Furger, M., Richard, A., Amato, F., Prevot, A. S. H., Baltensperger, U., Buchmann, B., and Gehrig, R.: PM_{10} emission factors for non-exhaust particles generated by road traffic in an urban street canyon and along a freeway in Switzerland, Atmos. Environ., 44, 2330–2340, 2010.

Canonaco, F., Crippa, M., Slowik, J. G., Baltensperger, U., and Prévôt, A. S. H.: SoFi, an IGOR-based interface for the efficient use of the generalized multilinear engine (ME-2) for the source apportionment: ME-2 application to aerosol mass spectrometer data, Atmos. Meas. Tech., 6, 3649–3661, doi:10.5194/amt-6-3649-2013, 2013.

Title Page

Abstract | Introduction

Conclusions | References

Tables | Figures

|◄ | ►|

◄ | ►

Back | Close

Full Screen / Esc

Printer-friendly Version

Interactive Discussion

Charron, A. and Harrison, R. M.: Fine ($PM_{2.5}$) and coarse ($PM_{2.5-10}$) particulate matter on a heavily trafficked London highway: sources and processes, Environ. Sci. Technol., 39, 7768–7776, doi:10.1021/es050462i, 2005.

Charron, A., Harrison, R. M., and Quincey, P.: What are the sources and conditions responsible for exceedences of the 24 h PM_{10} limit value (50 µg m^{-3}) at a heavily trafficked London site?, Atmos. Environ., 41, 1960–1975, 2007.

Crippa, M., DeCarlo, P. F., Slowik, J. G., Mohr, C., Heringa, M. F., Chirico, R., Poulain, L., Freutel, F., Sciare, J., Cozic, J., Di Marco, C. F., Elsasser, M., Nicolas, J. B., Marchand, N., Abidi, E., Wiedensohler, A., Drewnick, F., Schneider, J., Borrmann, S., Nemitz, E., Zimmermann, R., Jaffrezo, J.-L., Prévôt, A. S. H., and Baltensperger, U.: Wintertime aerosol chemical composition and source apportionment of the organic fraction in the metropolitan area of Paris, Atmos. Chem. Phys., 13, 961–981, doi:10.5194/acp-13-961-2013, 2013.

DeCarlo, P. F., Kimmel, J. R., Trimborn, A., Northway, M. J., Jayne, J. T., Aiken, A. C., Gonin, M., Fuhrer, K., Horvath, T., Docherty, K. S., Worsnop, D. R., and Jimenez, J. L.: Field-deployable, high-resolution, time-of-flight aerosol mass spectrometer, Anal. Chem., 78, 8281–8289, doi:10.1021/ac061249n, 2006.

Dockery, D. W. and Pope, C. A., III: Acute respiratory effects of particulate air pollution, in: Annual Review of Public Health, edited by: Omenn, G. S., Annual Review of Public Health, Annual Reviews Inc., P.O. Box 10139, 4139 El Camino Way, Palo Alto, California 94306, USA, 107–132, 1994.

Dore, C. J., Goodwin, J. W. L., Watterson, J. D., Murrels, T. P., Passant, N. R., Hobson, M. M., Haigh, K. E., Baggott, S. L., Pye, S. T., Coleman, P. J., and King, K. R.: UK Emissions of Air Pollutants 1970 to 2001, National Atmospheric Emissions Inventory, London, UK, 2003.

Flechsig, U., Jaggi, A., Spielmann, S., Padmore, H. A., and MacDowell, A. A.: The optics beamline at the Swiss Light Source, Nucl. Instrum. Meth. A, 609, 281–285, 2009.

Formenti, P., Prati, P., Zucchiatti, A., Lucarelli, F., and Mando, P. A.: Aerosol study in the town of Genova with a PIXE analysis, Nucl. Instrum. Meth. B, 113, 359–362, 1996.

Fowler, D. and Smith, R.: Spatial and Temporal Variability in the Deposition of Acidifying Species in the UK Between 1986 and 1997, Department of Environment Food and Rural Affairs, London, UK, 2000.

Franklin, M., Koutrakis, P., and Schwartz, J.: The role of particle composition on the association between $PM_{2.5}$ and mortality, Epidemiology, 19, 680–689, doi:10.1097/EDE.0b013e3181812bb7, 2008.

Freutel, F., Schneider, J., Drewnick, F., von der Weiden-Reinmüller, S.-L., Crippa, M., Prévôt, A. S. H., Baltensperger, U., Poulain, L., Wiedensohler, A., Sciare, J., Sarda-Estève, R., Burkhart, J. F., Eckhardt, S., Stohl, A., Gros, V., Colomb, A., Michoud, V., Doussin, J. F., Borbon, A., Haeffelin, M., Morille, Y., Beekmann, M., and Borrmann, S.: Aerosol particle measurements at three stationary sites in the megacity of Paris during summer 2009: meteorology and air mass origin dominate aerosol particle composition and size distribution, Atmos. Chem. Phys., 13, 933–959, doi:10.5194/acp-13-933-2013, 2013.

Gotschi, T., Hazenkamp-Von Arxb, M. E., Heinrich, J., Bono, R., Burney, P., Forsberg, B., Jarvis, D., Maldonado, J., Norback, D., Stern, W. B., Sunyer, J., Toren, K., Verlato, G., Villani, S., and Kunzli, N.: Elemental composition and reflectance of ambient fine particles at 21 European locations, Atmos. Environ., 39, 5947–5958, 2005.

Hammond, D. M., Dvonch, J. T., Keeler, G. J., Parker, E. A., Kamal, A. S., Barres, J. A., Yip, F. Y., and Brakefield-Caldwell, W.: Sources of ambient fine particulate matter at two community sites in Detroit, Michigan, Atmos. Environ., 42, 720–732, 2008.

Harrison, R. M. and Jones, A. M.: Multisite study of particle number concentrations in urban air, Environ. Sci. Technol., 39, 6063–6070, doi:10.1021/es040541e, 2005.

Harrison, R. M., Yin, J., Mark, D., Stedman, J., Appleby, R. S., Booker, J., and Moorcroft, S.: Studies of the coarse particle (2.5–10 μm) component in UK urban atmospheres, Atmos. Environ., 35, 3667–3679, 2001.

Harrison, R. M., Stedman, J., and Derwent, D.: New Directions: why are PM_{10} concentrations in Europe not falling?, Atmos. Environ., 42, 603–606, 2008.

Harrison, R. M., Beddows, D. C. S., and Dall'Osto, M.: PMF analysis of wide-range particle size spectra collected on a major highway, Environ. Sci. Technol., 45, 5522–5528, 2011.

Harrison, R. M., Dall'Osto, M., Beddows, D. C. S., Thorpe, A. J., Bloss, W. J., Allan, J. D., Coe, H., Dorsey, J. R., Gallagher, M., Martin, C., Whitehead, J., Williams, P. I., Jones, R. L., Langridge, J. M., Benton, A. K., Ball, S. M., Langford, B., Hewitt, C. N., Davison, B., Martin, D., Petersson, K. F., Henshaw, S. J., White, I. R., Shallcross, D. E., Barlow, J. F., Dunbar, T., Davies, F., Nemitz, E., Phillips, G. J., Helfter, C., Di Marco, C. F., and Smith, S.: Atmospheric chemistry and physics in the atmosphere of a developed megacity (London): an overview of the REPARTEE experiment and its conclusions, Atmos. Chem. Phys., 12, 3065–3114, doi:10.5194/acp-12-3065-2012, 2012a.

Harrison, R. M., Jones, A. M., Gietl, J., Yin, J., and Green, D. C.: Estimation of the contributions of brake dust, tire wear, and resuspension to nonexhaust traffic particles derived from at-

mospheric measurements, Environ. Sci. Technol., 46, 6523–6529, doi:10.1021/es300894r, 2012b.

Harrison, R. M., Laxen, D., Moorcroft, S., and Laxen, K.: Processes affecting concentrations of fine particulate matter (PM$_{2.5}$) in the UK atmosphere, Atmos. Environ., 46, 115–124, 2012c.

5   Janssen, N. A. H., Van Mansom, D. F. M., Van Der Jagt, K., Harssema, H., and Hoek, G.: Mass concentration and elemental composition of airborne particulate matter at street and background locations, Atmos. Environ., 31, 1185–1193, 1997.

Jones, A. M., Harrison, R. M., and Baker, J.: The wind speed dependence of the concentrations of airborne particulate matter and NO$_x$, Atmos. Environ., 44, 1682–1690, 2010.

10   Jones, A. R., Thomson, D. J., Hort, M., and Devenish, B.: The UK Met Office's next-generation atmospheric dispersion model, NAME III, in: Air Pollution Modeling and its Application XVII, edited by: Borrego, C. and Norman, A.-L., Springer US, New York, NY, USA, 744 pp., 2007

Kelly, F. J. and Fussell, J. C.: Size, source and chemical composition as determinants of toxicity attributable to ambient particulate matter, Atmos. Environ., 60, 504–526, 2012.

15   Lee, D. S., Garland, J. A., and Fox, A. A.: Atmospheric concentrations of trace elements in urban areas of the UK, Atmos. Environ., 28, 2691–2713, 1994.

Lin, C. C., Chen, S. J., Huang, K. L., Hwang, W. I., Chang-Chien, G. P., and Lin, W. Y.: Characteristics of metals in nano/ultrafine/fine/coarse particles collected beside a heavily trafficked road, Environ. Sci. Technol., 39, 8113–8122, 2005.

20   Lucarelli, F., Mando, P. A., Nava, S., Valerio, M., Prati, P., and Zucchiatti, A.: Elemental composition of urban aerosol collected in Florence, Italy, Environ. Monit. Assess., 65, 165–173, 2000.

Maenhaut, W.: "Global Change" related and other atmospheric aerosol research at the University of Gent, and the role of PIXE therein, Nucl. Instrum. Meth. B, 109, 419–428, 1996.

25   Mavrogianni, A., Davies, M., Batty, M., Belcher, S. E., Bohnenstengel, S. I., Carruthers, D., Chalabi, Z., Croxford, B., Demanuele, C., Evans, S., Giridharan, R., Hacker, J. N., Hamilton, I., Hogg, C., Hunt, J., Kolokotroni, M., Martin, C., Milner, J., Rajapaksha, I., Ridley, I., Steadman, J. P., Stocker, J., Wilkinson, P., and Ye, Z.: The comfort, energy and health implications of London's urban heat island, Build Serv. Eng. Res. T., 32, 35–52, 30   doi:10.1177/0143624410394530, 2011.

Mazzei, F., Lucarelli, F., Nava, S., Prati, P., Valli, G., and Vecchi, R.: A new methodological approach: the combined use of two-stage streaker samplers and optical particle counters for the characterization of airborne particulate matter, Atmos. Environ., 41, 5525–5535, 2007.

Minguillón, M. C., Cirach, M., Hoek, G., Brunekreef, B., Tsai, M., de Hoogh, K., Jedynska, A., Kooter, I. M., Nieuwenhuijsen, M., and Querol, X.: Spatial variability of trace elements and sources for improved exposure assessment in Barcelona, Atmos. Environ., 89, 268–281, 2014.

5 Moffet, R. C., Desyaterik, Y., Hopkins, R. J., Tivanski, A. V., Gilles, M. K., Wang, Y., Shutthanan-dan, V., Molina, L. T., Abraham, R. G., Johnson, K. S., Mugica, V., Molina, M. J., Laskin, A., and Prather, K. A.: Characterization of aerosols containing Zn, Pb, and Cl from an industrial region of Mexico City, Environ. Sci. Technol., 42, 7091–7097, 2008.

Mohr, C., Lopez-Hilfiker, F. D., Zotter, P., Prévôt, A. S. H., Xu, L., Ng, N. L., Herndon, S. C.,
10 Williams, L. R., Franklin, J. P., Zahniser, M. S., Worsnop, D. R., Knighton, W. B., Aiken, A. C., Gorkowski, K. J., Dubey, M. K., Allan, J. D., and Thornton, J. A.: Contribution of nitrated phenols to wood burning brown carbon light absorption in Detling, United Kingdom during winter time, Environ. Sci. Technol., 47, 6316–6324, doi:10.1021/es400683v, 2013.

Moreno, T., Karanasiou, A., Amato, F., Lucarelli, F., Nava, S., Calzolai, G., Chiari, M.,
15 Coz, E., Artinano, B., Lumbreras, J., Borge, R., Boldo, E., Linares, C., Alastuey, A., Querol, X., and Gibbons, W.: Daily and hourly sourcing of metallic and mineral dust in urban air contaminated by traffic and coal-burning emissions, Atmos. Environ., 68, 33–44, doi:10.1016/j.atmosenv.2012.11.037, 2013.

Nolte, C. G., Bhave, P. V., Arnold, J. R., Dennis, R. L., Zhang, K. M., and Wexler, A. S.: Mod-
20 eling urban and regional aerosols – application of the CMAQ-UCD Aerosol Model to Tampa, a coastal urban site, Atmos. Environ., 42, 3179–3191, 2008.

Paatero, P.: The multilinear engine – a table-driven, least squares program for solving multilinear problems, including the n-way parallel factor analysis model, J. Comput. Graph. Stat., 8, 854–888, doi:10.1080/10618600.1999.10474853, 1999.

25 Putaud, J. P., Van Dingenen, R., Alastuey, A., Bauer, H., Birmili, W., Cyrys, J., Flentje, H., Fuzzi, S., Gehrig, R., Hansson, H. C., Harrison, R. M., Herrmann, H., Hitzenberger, R., Hüglin, C., Jones, A. M., Kasper-Giebl, A., Kiss, G., Kousa, A., Kuhlbusch, T. A. J., Löschau, G., Maenhaut, W., Molnar, A., Moreno, T., Pekkanen, J., Perrino, C., Pitz, M., Puxbaum, H., Querol, X., Rodriguez, S., Salma, I., Schwarz, J., Smolik, J., Schneider, J.,
30 Spindler, G., ten Brink, H., Tursic, J., Viana, M., Wiedensohler, A., and Raes, F.: A European aerosol phenomenology – 3: Physical and chemical characteristics of particulate matter from 60 rural, urban, and kerbside sites across Europe, Atmos. Environ., 44, 1308–1320, 2010.

Title Page

Abstract	Introduction
Conclusions	References
Tables	Figures

◀ | ▶

◀ | ▶

Back | Close

Full Screen / Esc

Printer-friendly Version

Interactive Discussion

Querol, X., Viana, M., Alastuey, A., Amato, F., Moreno, T., Castillo, S., Pey, J., de la Rosa, J., Sánchez de la Campa, A., Artíñano, B., Salvador, P., García Dos Santos, S., Fernández-Patier, R., Moreno-Grau, S., Negral, L., Minguillón, M. C., Monfort, E., Gil, J. I., Inza, A., Ortega, L. A., Santamaría, J. M., and Zabalza, J.: Source origin of trace elements in PM from regional background, urban and industrial sites of Spain, Atmos. Environ., 41, 7219–7231, 2007.

Reche, C., Moreno, T., Amato, F., Viana, M., van Drooge, B. L., Chuang, H.-C., Bérubé, K., Jones, T., Alastuey, A., and Querol, X.: A multidisciplinary approach to characterise exposure risk and toxicological effects of PM_{10} and $PM_{2.5}$ samples in urban environments, Ecotox. Environ. Safe., 78, 327–335, 2012.

Richard, A., Bukowiecki, N., Lienemann, P., Furger, M., Fierz, M., Minguillón, M. C., Weideli, B., Figi, R., Flechsig, U., Appel, K., Prévôt, A. S. H., and Baltensperger, U.: Quantitative sampling and analysis of trace elements in atmospheric aerosols: impactor characterization and Synchrotron-XRF mass calibration, Atmos. Meas. Tech., 3, 1473–1485, doi:10.5194/amt-3-1473-2010, 2010.

Richard, A., Gianini, M. F. D., Mohr, C., Furger, M., Bukowiecki, N., Minguillón, M. C., Lienemann, P., Flechsig, U., Appel, K., DeCarlo, P. F., Heringa, M. F., Chirico, R., Baltensperger, U., and Prévôt, A. S. H.: Source apportionment of size and time resolved trace elements and organic aerosols from an urban courtyard site in Switzerland, Atmos. Chem. Phys., 11, 8945–8963, doi:10.5194/acp-11-8945-2011, 2011.

Salcedo, D., Laskin, A., Shutthanandan, V., and Jimenez, J. L.: Feasibility of the detection of trace elements in particulate matter using online high-resolution aerosol mass spectrometry, Aerosol Sci. Tech., 46, 1187–1200, doi:10.1080/02786826.2012.701354, 2012.

Sole, V. A., Papillon, E., Cotte, M., Walter, P., and Susini, J.: A multiplatform code for the analysis of energy-dispersive X-ray fluorescence spectra, Spectrochim. Acta B, 62, 63–68, 2007.

Theodosi, C., Grivas, G., Zarmpas, P., Chaloulakou, A., and Mihalopoulos, N.: Mass and chemical composition of size-segregated aerosols (PM_1, $PM_{2.5}$, PM_{10}) over Athens, Greece: local versus regional sources, Atmos. Chem. Phys., 11, 11895–11911, doi:10.5194/acp-11-11895-2011, 2011.

Turóczi, B., Hoffer, A., Tóth, Á., Kováts, N., Ács, A., Ferincz, Á., Kovács, A., and Gelencsér, A.: Comparative assessment of ecotoxicity of urban aerosol, Atmos. Chem. Phys., 12, 7365–7370, doi:10.5194/acp-12-7365-2012, 2012.

Title Page

Abstract | Introduction

Conclusions | References

Tables | Figures

◀ | ▶

◀ | ▶

Back | Close

Full Screen / Esc

Printer-friendly Version

Interactive Discussion

Van Espen, P., Janssens, K., and Nobels, J.: AXIL-PC, software for the analysis of complex X-ray spectra, Chemometr. Intell. Lab., 1, 109–114, 1986.

Viana, M., Kuhlbusch, T. A. J., Querol, X., Alastuey, A., Harrison, R. M., Hopke, P. K., Winiwarter, W., Vallius, A., Szidat, S., Prevot, A. S. H., Hueglin, C., Bloemen, H., Wahlin, P., Vecchi, R., Miranda, A. I., Kasper-Giebl, A., Maenhaut, W., and Hitzenberger, R.: Source apportionment of particulate matter in Europe: a review of methods and results, J. Aerosol Sci., 39, 827–849, doi:10.1016/j.jaerosci.2008.05.007, 2008.

Weijers, E. P., Schaap, M., Nguyen, L., Matthijsen, J., Denier van der Gon, H. A. C., ten Brink, H. M., and Hoogerbrugge, R.: Anthropogenic and natural constituents in particulate matter in the Netherlands, Atmos. Chem. Phys., 11, 2281–2294, doi:10.5194/acp-11-2281-2011, 2011.

Witt, M. L. I., Meheran, N., Mather, T. A., de Hoog, J. C. M., and Pyle, D. M.: Aerosol trace metals, particle morphology and total gaseous mercury in the atmosphere of Oxford, UK, Atmos. Environ., 44, 1524–1538, doi:10.1016/j.atmosenv.2010.01.008, 2010.

Wood, C. R., Lacser, A., Barlow, J. F., Padhra, A., Belcher, S. E., Nemitz, E., Helfter, C., Famulari, D., and Grimmond, C. S. B.: Turbulent flow at 190 m height above London during 2006–2008: a climatology and the applicability of similarity theory, Bound.-Lay. Meteorol., 137, 77–96, doi:10.1007/s10546-010-9516-x, 2010.

Xiao, Z. H., Shao, L. Y., Zhang, N., Wang, J., and Wang, J. Y.: Heavy metal compositions and bioreactivity of airborne PM_{10} in a valley-shaped city in northwestern China, Aerosol Air Qual. Res., 13, 1116–1125, doi:10.4209/aaqr.2012.10.0287, 2013.

Zhou, J. A., Ito, K., Lall, R., Lippmann, M., and Thurston, G.: Time-series analysis of mortality effects of fine particulate matter components in Detroit and Seattle, Environ. Health Persp., 119, 461–466, doi:10.1289/ehp.1002613, 2011.

Zhou, Y. and Levy, J. I.: The impact of urban street canyons on population exposure to traffic-related primary pollutants, Atmos. Environ., 42, 3087–3098, 2008.

Title Page

Abstract | Introduction

Conclusions | References

Tables | Figures

|◀ | ▶|

◀ | ▶

Back | Close

Full Screen / Esc

Printer-friendly Version

Interactive Discussion

Table 1. Measurement campaign details.

Site	Start/End date	Site type	Sampling time	Inlet height	Sampling platform
MR	11 Jan–14 Feb 2012	kerbside	2 h	4 m	container at 1 m from road
NK	11 Jan–9 Feb 2012	urban background	2 h	4 m	container
DE	17 Jan–13 Feb 2012	rural	2 h	1.5 m	grass field

Table 2. Mean, median and 25–75th percentile trace element concentrations ($ng\,m^{-3}$) for $PM_{10-2.5}$, $PM_{2.5-1.0}$ and $PM_{1.0-0.3}$ at MR, NK and DE.

Marylebone Road

Element	$PM_{10-2.5}$ mean	median	25th perc	75th perc	$PM_{2.5-1.0}$ mean	median	25th perc	75th perc	$PM_{1.0-0.3}$ mean	median	25th perc	75th perc
Na	983.4	919.5	482.8	1400.5	394.3	276.2	174.0	515.0	122.3	70.0	47.3	123.2
Mg	154.7	141.6	97.5	201.2	70.8	55.2	37.7	95.8	28.4	23.7	17.2	33.4
Al	135.9	109.4	74.1	169.4	59.0	53.2	41.9	71.6	22.3	20.4	15.4	27.7
Si	292.7	226.4	138.5	376.2	95.3	76.0	44.1	123.0	28.3	23.3	14.1	36.2
P	16.2	14.4	9.8	20.8	6.3	5.6	3.6	8.3	4.5	3.4	2.3	6.0
S	122.9	109.0	77.3	151.7	59.3	49.9	35.5	74.8	178.0	75.6	34.5	259.6
Cl	968.4	844.5	358.7	1426.2	265.5	134.1	39.1	401.0	102.9	32.0	6.5	131.0
K	42.0	37.3	26.7	50.9	14.9	12.6	8.4	19.2	15.9	10.7	7.1	20.7
Ca	228.7	172.7	105.9	300.6	65.6	46.5	28.3	84.7	18.2	13.5	8.1	22.5
Ti	7.4	5.8	3.3	10.0	2.4	1.8	1.1	3.3	0.8	0.6	0.4	1.0
V	2.2	1.9	1.1	2.9	0.8	0.7	0.4	1.1	0.4	0.3	0.2	0.5
Cr	6.2	3.6	2.0	5.9	1.7	1.4	0.9	2.3	0.6	0.5	0.3	0.8
Mn	9.4	7.6	4.6	12.2	3.8	3.3	2.4	4.9	1.8	1.5	1.0	2.2
Fe	690.0	599.0	345.4	925.7	244.1	212.8	128.0	326.9	85.0	71.4	41.1	114.8
Ni	2.1	0.6	0.4	1.0	0.4	0.3	0.2	0.4	0.2	0.1	0.1	0.3
Cu	26.2	23.0	12.7	33.6	9.4	8.1	4.5	12.4	3.4	2.7	1.6	4.6
Zn	11.1	9.0	5.3	14.2	4.3	3.6	2.0	5.6	4.6	3.0	1.7	6.4
Br	3.0	2.4	1.4	3.9	1.0	0.8	0.5	1.2	2.0	1.2	0.6	2.7
Sr	1.4	1.2	0.8	1.7	0.5	0.4	0.3	0.7	0.2	0.2	0.1	0.3
Zr	3.0	2.1	1.1	3.8	1.2	0.8	0.5	1.5	0.4	0.3	0.2	0.6
Mo	3.8	2.7	1.4	4.8	1.4	1.2	0.7	1.8	0.6	0.5	0.3	0.7
Sn	4.9	4.0	2.3	6.5	1.9	1.7	1.0	2.6	0.8	0.7	0.4	1.2
Sb	4.1	3.1	1.8	5.5	1.5	1.2	0.7	1.9	0.7	0.5	0.3	0.9
Ba	22.7	18.8	10.9	30.6	8.8	7.7	4.5	11.6	3.4	2.6	1.6	4.5
Pb	2.1	1.4	0.8	2.3	0.9	0.6	0.3	1.1	1.8	0.9	0.4	2.2

Table 2. Continued.

North Kensington Element	PM$_{10-2.5}$ mean	median	25th perc	75th perc	PM$_{2.5-1.0}$ mean	median	25th perc	75th perc	PM$_{1.0-0.3}$ mean	median	25th perc	75th perc
Na	640.3	550.7	290.5	966.0	399.6	281.8	182.4	529.8	125.2	61.7	42.8	138.2
Mg	84.6	74.0	44.8	123.9	64.4	49.9	35.7	86.2	24.1	17.9	10.6	30.2
Al	50.9	43.1	27.1	67.2	45.2	41.9	30.6	52.9	17.3	15.3	12.4	20.3
Si	97.2	79.0	39.7	121.3	57.6	46.2	25.8	78.2	15.8	11.2	6.6	19.4
P	6.5	5.6	3.3	9.0	4.0	3.5	2.1	5.0	3.1	2.1	1.3	3.8
S	62.4	55.5	37.5	84.1	49.7	39.8	28.1	60.4	158.6	74.5	34.8	192.3
Cl	533.6	420.3	135.5	860.2	243.0	96.4	22.8	353.1	80.7	12.6	3.2	84.3
K	21.8	19.3	12.5	30.1	12.8	10.9	7.4	17.7	13.7	9.1	5.5	16.7
Ca	90.5	68.7	39.7	112.1	44.5	33.1	18.7	53.5	10.6	7.7	4.4	12.6
Ti	2.7	1.7	0.9	3.1	1.5	1.1	0.5	2.1	0.4	0.3	0.1	0.5
V	0.6	0.4	0.2	0.7	0.3	0.2	0.1	0.4	0.2	0.1	0.1	0.3
Cr	1.2	0.7	0.4	1.5	0.7	0.5	0.3	0.8	0.2	0.2	0.1	0.3
Mn	2.4	1.7	1.0	3.0	2.2	1.9	1.2	2.6	1.1	0.8	0.5	1.1
Fe	163.1	120.3	69.6	201.7	92.9	68.5	36.8	118.4	28.5	17.7	9.2	33.0
Ni	0.4	0.2	0.1	0.4	0.2	0.1	0.1	0.2	0.1	0.1	0.0	0.1
Cu	4.9	3.6	1.8	6.4	3.7	2.6	1.5	4.7	1.3	0.8	0.5	1.5
Zn	2.9	1.9	1.0	3.4	2.2	1.6	0.8	2.9	3.2	1.9	0.9	4.4
Br	1.3	1.0	0.4	1.8	0.8	0.6	0.4	1.1	2.0	1.3	0.7	2.4
Sr	0.5	0.4	0.2	0.6	0.3	0.3	0.2	0.4	0.2	0.1	0.1	0.2
Zr	0.4	0.2	0.0	0.4	0.4	0.2	0.1	0.4	0.1	0.1	0.0	0.2
Mo	0.8	0.3	0.2	0.7	0.5	0.3	0.2	0.7	0.3	0.2	0.1	0.3
Sn	0.7	0.4	0.2	0.8	0.6	0.4	0.2	0.8	0.4	0.3	0.1	0.5
Sb	0.5	0.3	0.1	0.6	0.5	0.4	0.2	0.6	0.4	0.3	0.1	0.4
Ba	4.1	2.1	1.0	4.2	3.0	2.1	1.1	3.9	1.5	1.1	0.6	1.9
Pb	0.3	0.2	0.0	0.4	0.5	0.3	0.1	0.7	1.7	0.9	0.4	2.0

Table 2. Continued.

Detling Element	PM$_{10-2.5}$ mean	median	25th perc	75th perc	PM$_{2.5-1.0}$ mean	median	25th perc	75th perc	PM$_{1.0-0.3}$ mean	median	25th perc	75th perc
Na	344.4	253.2	46.5	550.2	215.1	122.2	43.8	267.0	107.2	52.9	23.7	138.9
Mg	44.2	35.0	9.5	63.4	35.2	24.7	7.7	48.2	27.0	15.9	6.3	31.9
Al	26.4	24.2	12.4	37.3	35.1	35.5	19.9	47.3	16.6	14.1	9.4	21.6
Si	58.4	47.2	24.4	74.9	30.2	24.0	10.8	44.2	11.3	8.9	4.7	16.3
P	3.6	2.8	1.2	4.6	1.9	1.6	0.8	2.6	3.3	1.8	0.9	4.2
S	36.4	31.6	6.5	48.2	32.2	28.2	12.8	44.7	212.3	63.6	27.3	235.6
Cl	217.8	46.5	3.1	347.8	123.3	8.7	2.3	136.2	86.6	10.1	3.3	78.1
K	12.3	10.5	3.1	15.8	7.6	6.7	2.5	11.1	21.0	7.7	3.6	20.9
Ca	34.4	26.5	10.2	42.6	19.2	13.2	5.3	22.4	12.3	4.7	2.6	8.2
Ti	0.9	0.5	0.2	1.3	0.7	0.4	0.2	0.9	0.2	0.2	0.1	0.3
V	0.2	0.1	0.1	0.2	0.1	0.1	0.1	0.2	0.2	0.1	0.0	0.3
Cr	3.9	0.9	0.3	2.9	0.8	0.4	0.2	0.6	0.2	0.2	0.1	0.3
Mn	1.8	0.6	0.3	1.3	1.5	1.6	0.7	2.0	1.3	0.8	0.4	1.2
Fe	55.4	37.0	20.0	66.5	25.4	20.5	11.0	35.8	10.6	8.1	4.4	13.5
Ni	4.3	0.7	0.2	2.7	0.8	0.2	0.1	0.4	3.3	0.2	0.1	0.6
Cu	1.4	0.8	0.3	1.8	1.0	0.8	0.5	1.3	1.1	0.5	0.2	0.9
Zn	3.4	0.9	0.4	1.9	1.4	0.7	0.4	1.7	5.7	1.9	0.6	7.0
Br	1.3	0.5	0.2	1.5	0.5	0.3	0.1	0.6	2.7	1.3	0.6	3.1
Sr	0.3	0.2	0.1	0.3	0.1	0.1	0.0	0.2	0.1	0.1	0.0	0.1
Zr	0.0	0.0	−0.1	0.1	0.1	0.1	0.0	0.1	0.0	0.0	0.0	0.1
Mo	2.2	0.2	0.1	0.7	0.3	0.1	0.0	0.2	0.2	0.1	0.0	0.2
Sn	0.3	0.1	0.0	0.3	0.2	0.1	0.0	0.2	0.3	0.2	0.1	0.4
Sb	0.3	0.1	0.0	0.2	0.1	0.1	0.0	0.1	0.3	0.1	0.0	0.4
Ba	1.3	0.6	0.3	1.1	0.6	0.4	0.2	0.8	0.6	0.4	0.1	0.8
Pb	0.4	0.2	0.0	0.3	0.3	0.2	0.1	0.4	1.8	0.6	0.2	2.1
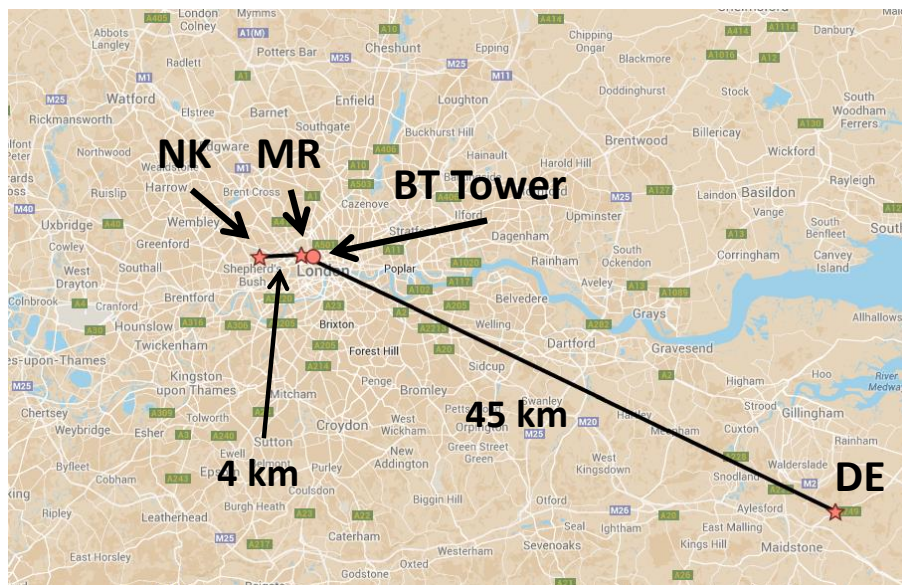
Figure 1. Map of south eastern UK. Indicated are the sampling sites MR (kerbside site Maryle-bone Road), NK (urban background site North Kensington), DE (rural site Detling), and the elevated BT Tower site for meteorological measurements (adapted from Google Maps).
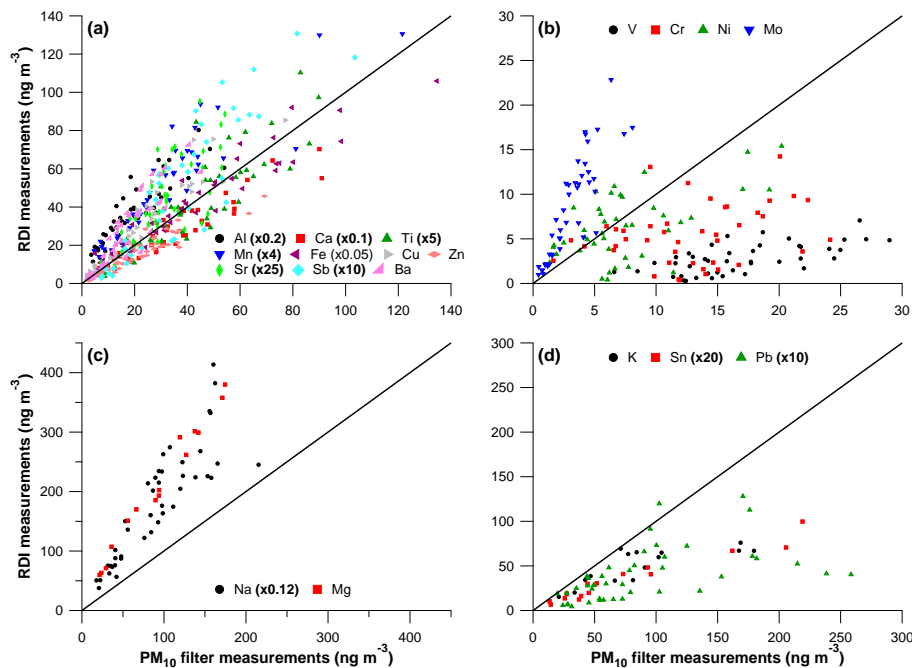
Figure 2. Total PM_{10} element mass concentrations measured by the RDI (sum of $PM_{10-2.5}$, $PM_{2.5-1.0}$ and $PM_{1.0-0.3}$ fractions) at MR and NK averaged to 24 h vs. 24 h PM_{10} filter measurements of elements for **(a)** elements that agree within ±50 %, **(b)** elements with poor correlations, **(c)** elements with good correlations but a factor 2 higher with RDI, **(d)** other elements. The one-to-one line is added in black. See Supplement Table S2 for fit coefficients and Pearson's *R* values. Note that many elements are scaled to improve visualization.

Title Page

Abstract | Introduction

Conclusions | References

Tables | Figures

|◄ | ►|

◄ | ►

Back | Close

Full Screen / Esc

Printer-friendly Version

Interactive Discussion
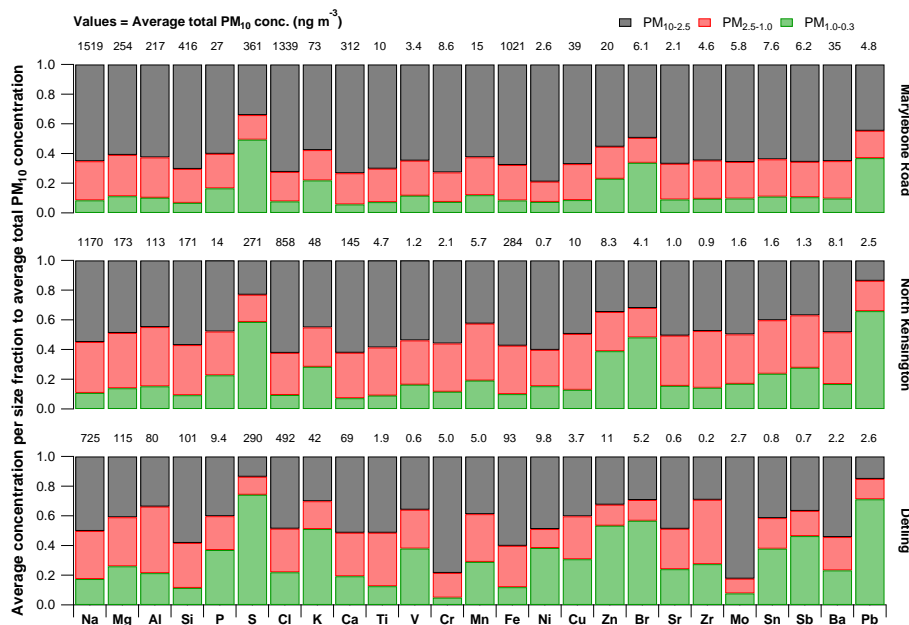
Figure 3. Relative contribution for trace elements in $PM_{10-2.5}$, $PM_{2.5-1.0}$ and $PM_{1.0-0.3}$ to total PM_{10} mean concentration per element at MR (top), NK (middle) and DE (bottom). Absolute mean total PM_{10} element concentrations are shown above each bar.
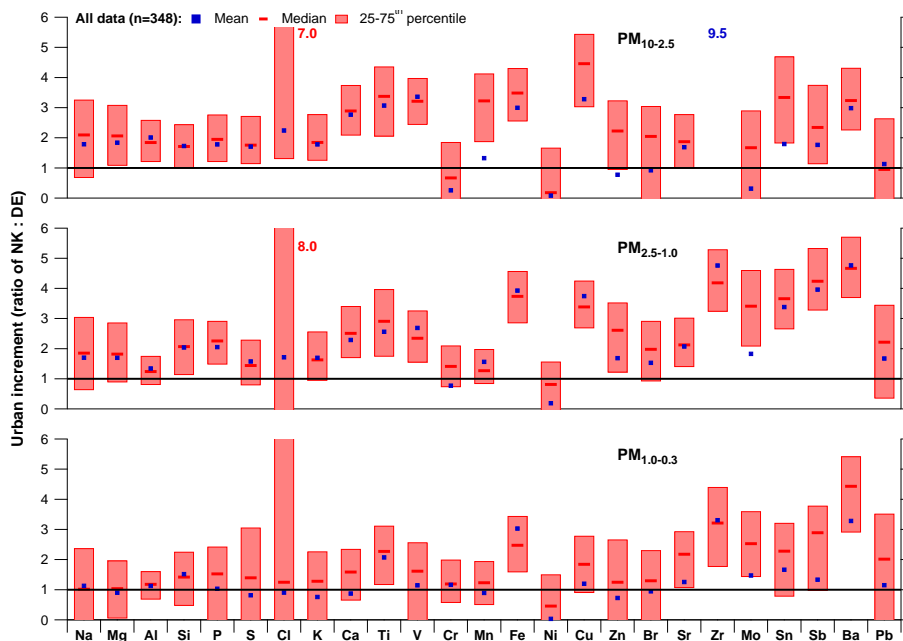
Figure 4. Mean, median and 25–75th percentile urban increment values for trace elements at NK relative to DE for $PM_{10-2.5}$ (top), $PM_{2.5-1.0}$ (middle) and $PM_{1.0-0.3}$ (bottom). Note that the median of Zr in $PM_{10-2.5}$ is below detection limit.
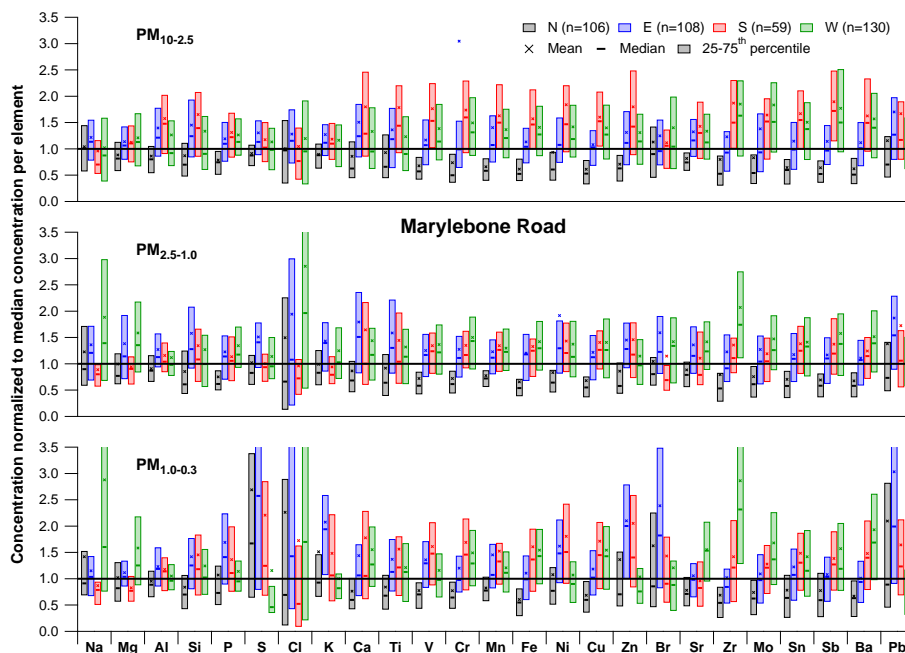
Figure 5. Mean, median and 25–75th percentile trace element concentrations at MR split in four wind direction sectors (N, E, S, W) normalized to the global median concentration per element for $PM_{10-2.5}$ (top), $PM_{2.5-1.0}$ (middle) and $PM_{1.0-0.3}$ (bottom). See Sect. 4.2.2 for the definition of the wind direction sectors.

Title Page

Abstract | Introduction

Conclusions | References

Tables | Figures

|◀ | ▶|

◀ | ▶

Back | Close

Full Screen / Esc

Printer-friendly Version

Interactive Discussion
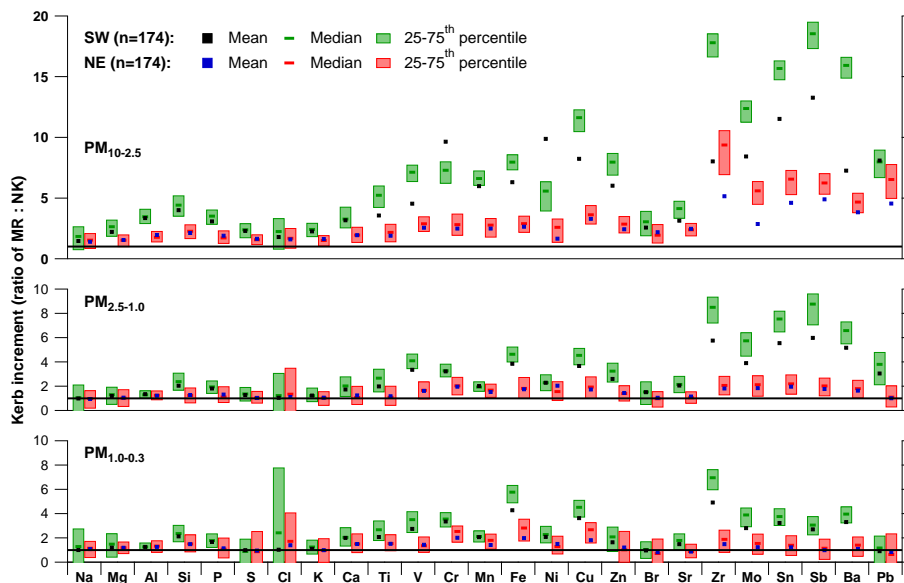
Figure 6. Mean, median and 25–75th percentile kerb increment values for trace elements at MR relative to NK for $PM_{10-2.5}$ (top), $PM_{2.5-1.0}$ (middle) and $PM_{1.0-0.3}$ (bottom) split in SW and NE wind sectors. See Sect. 4.2.2 for the definition of the wind direction sectors.
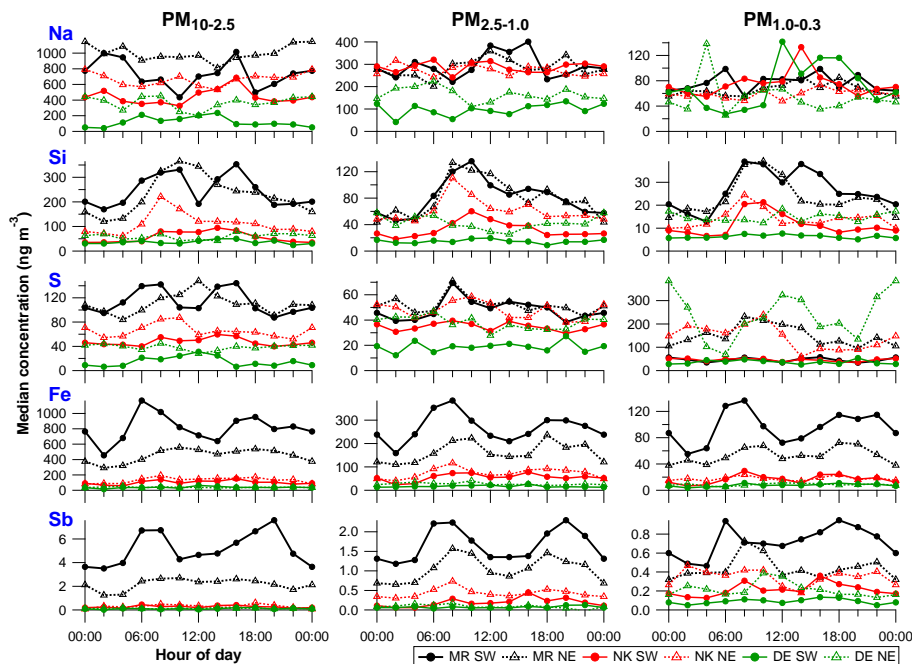
Figure 7. Diurnal cycles of 2 h median concentrations of Na, Si, S, Fe and Sb for $PM_{10-2.5}$ (left), $PM_{2.5-1.0}$ (middle) and $PM_{1.0-0.3}$ (right) at MR, NK, DE split in SW and NE wind sectors. See Sect. 4.2.2 for the definition of the wind direction sectors. Hour of day is start of 2 h sampling period, so 00:00 LT means sampling from 00:00 to 02:00 LT.
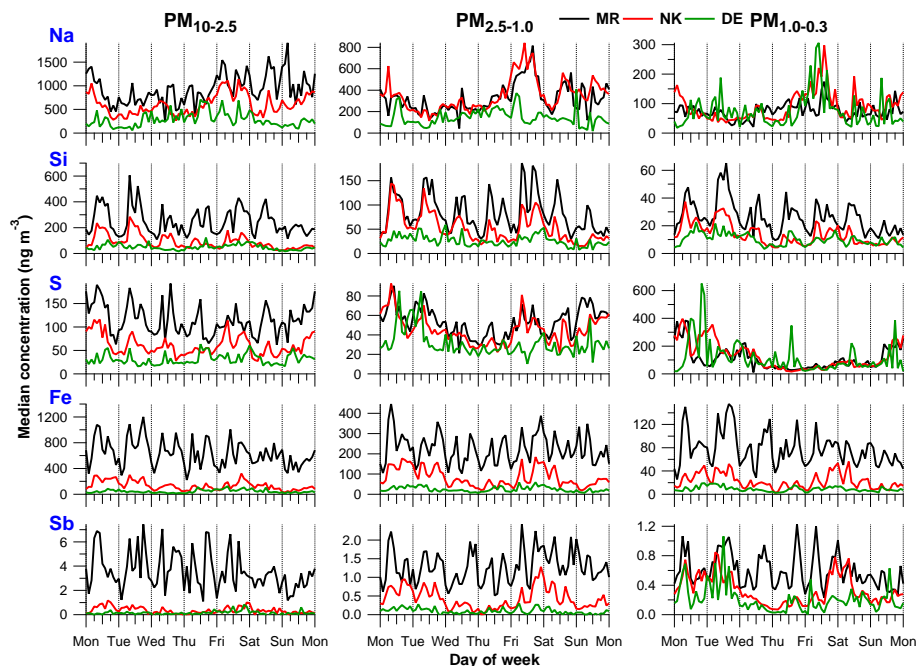
Figure 8. Weekly cycles of 2 h median concentrations of Na, Si, S, Fe and Sb for $PM_{10-2.5}$ (left), $PM_{2.5-1.0}$ (middle) and $PM_{1.0-0.3}$ (right) at MR, NK, DE.
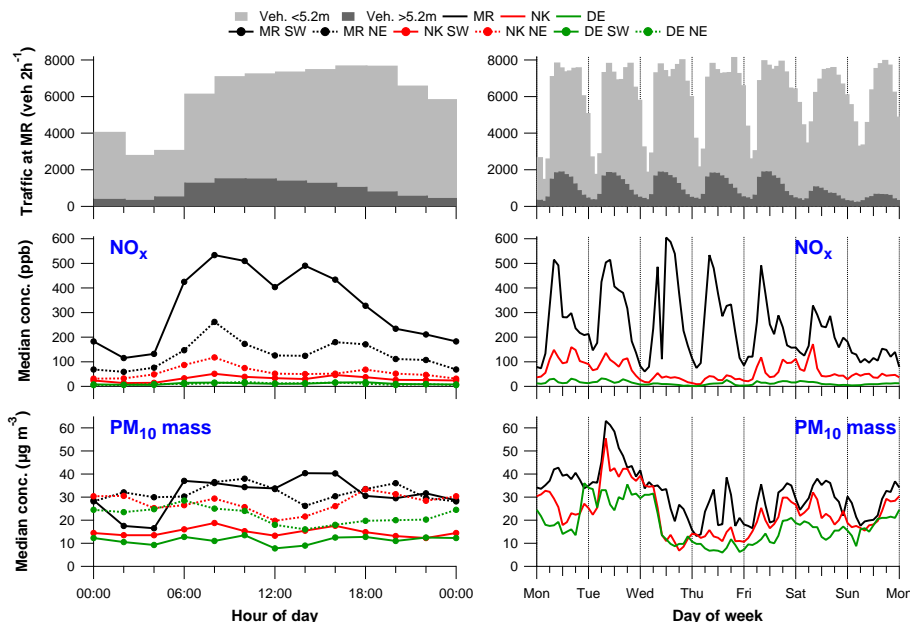
Figure 9. (top) Diurnal (left) and weekly (right) cycles of traffic flow at MR, (middle and bottom left) diurnal cycles of 2 h median NO_x and total PM_{10} mass concentrations at MR, NK and DE split in SW and NE wind sectors, and (middle and bottom right) weekly cycles of 2 h median NO_x and total PM_{10} mass concentrations at MR, NK and DE. See Sect. 4.2.2 for the definition of the wind direction sectors. Time stamp is start of 2 h averaging period, so 00:00 LT means averaging between 00:00 and 02:00 LT.
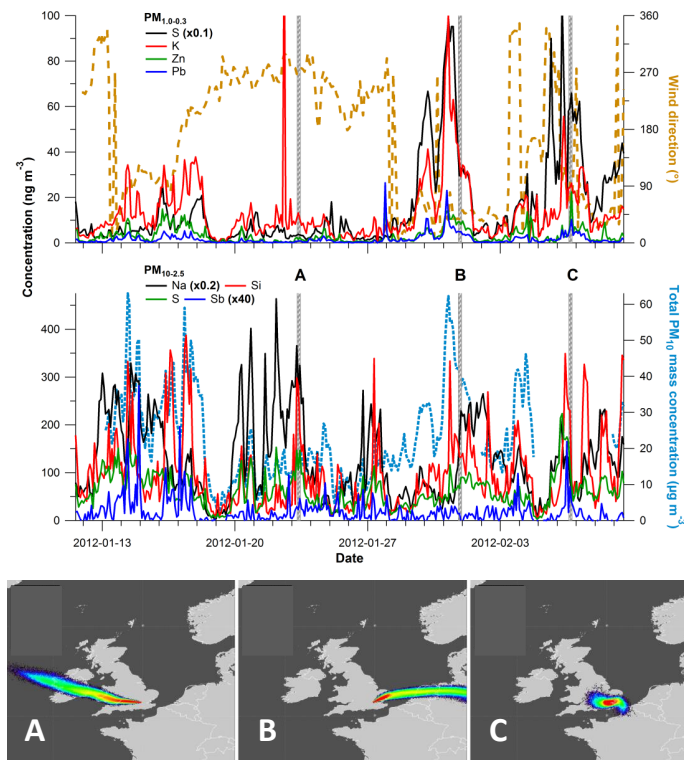
Figure 10. (top panel) Time series of (top left axis) $PM_{1.0-0.3}$ S, K, Zn and Pb concentrations at NK and (top right axis) wind direction from BT Tower, time series of (bottom left axis) $PM_{10-2.5}$ Na, Si, S and Sb concentrations at NK and (bottom right axis) total PM_{10} mass concentration at NK; (bottom panel) three NK footprints simulated with the NAME model corresponding to the vertical lines (A, B, C) indicated in the top panel. Trajectories are simulated for particles released from NK and followed back at 0–100 m a.g.l. for the previous 24 h at: **(A)** 23 January 2012 09:00 LT, **(B)** 31 January 2012 21:00 LT, **(C)** 6 February 2012 18:00 LT; particle concentrations increase from blue to red.

Title Page

Abstract | Introduction

Conclusions | References

Tables | Figures

|◄ | ►|

◄ | ►

Back | Close

Full Screen / Esc

Printer-friendly Version

Interactive Discussion